Politecnico di Torino

Department of Electronics and Telecommunications

Electronic properties of materials

Laboratory report

Monte Carlo simulation
for the study of electronic transport in semiconductors.

Supervisor: Prof. Francesco Bertazzi

Students:

Fabrizio Berritta	s258252
Kevin Montano	s263268

June 15, 2019

Contents

Introduction

The aim of the laboratory has been the development of a Monte Carlo simulation code for the study of electronic transport in GaAs. In the first chapter results of different scattering mechanism are discussed, among which *acoustic deformation potential, intervalley, polar optical phonons* and *ionized impurity scattering.*
These scattering mechanisms have been exploited to solve the Boltzmann Equation as addressed in the second chapter. At first, the mobility of GaAs as a function of temperature has been evaluated by means of the *relaxation time approximation.* Only acoustic deformation potential and ionized impurity scattering have been considered. In the second part, influence of the scatterings of the first chapter on the peak velocity, negative differential mobility, electron energy and noise diffusivity at 300 K has been studied using Monte Carlo simulations. At last, a simple Monte Carlo device simulation has been included to study the impact ionization coefficient in a bulk semiconductor.

Chapter 1

Scattering rates

Transport of electrons in material is mainly linked to their scattering properties. In this chapter different scatterings will be computed through `Matlab` simulations. Expressions for the rates always come from the *Fermi Golden Rule*, which should be applied case by case depending on the nature of the scattering perturbation.

1.1 Acoustic Deformation Potential

In the following, scattering rate related to acoustic deformation potential in the Γ valley is computed, both in inelastic and elastic case. Absorption and emission spectra are, in addition, studied for two different temperatures: $T = 300\,\mathrm{K}$ and $T = 77\,\mathrm{K}$.

Inelastic expression The inelastic acoustic scattering rate has been computed through `Matlab`, according to equation (1.1):

$$W_{\mathrm{aco}}(E_i) = \frac{\sqrt{m^*}(k_B T)^3 D_a^2}{2^{5/2}\pi\hbar^4 \nu_l^4 \rho \sqrt{\gamma(E_i)}} \cdot \begin{cases} (1+2\alpha E_i)\left[F_1(x_{2,a}) - F_1(x_{1,a})\right] + 2\alpha k_B T\left[F_2(x_{2,a}) - F_2(x_{1,a})\right] \\ (1+2\alpha E_i)\left[G_1(x_{2,e}) - G_1(x_{1,e})\right] - 2\alpha k_B T\left[G_2(x_{2,e}) - G_2(x_{1,e})\right] \end{cases} \tag{1.1}$$

where the two differentiated expressions are related to absorption rate (the first) and emission rate (the second). $F_1(x)$, $F_2(x)$, $G_1(x)$ and $G_2(x)$ are integral functions as shown in the reference notes [1].
Obtained results for the two different temperatures are depicted in Fig. 1.1 and 1.2.

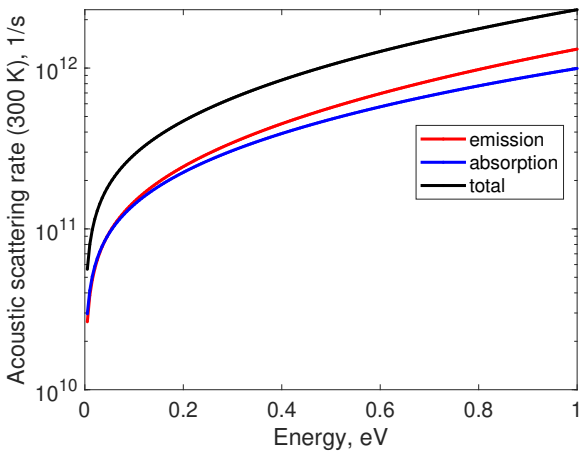

FIGURE 1.1: Acoustic inelastic rate for GaAs at T=300 K.

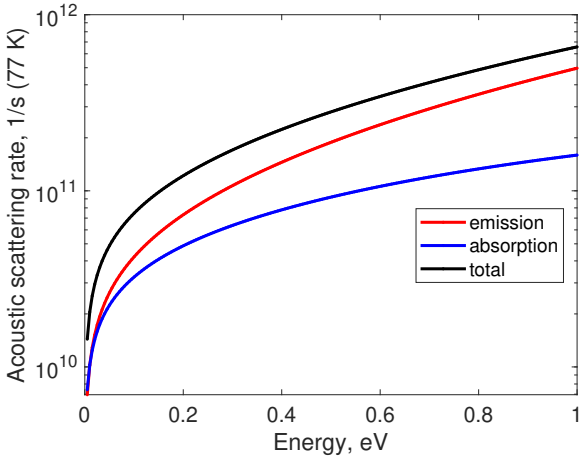

FIGURE 1.2: Acoustic inelastic rate for GaAs at T=77 K.

The comparison between the two temperatures is outlined in Fig. 1.3 and compared to literature data [2, Chapter 2] in Fig. 1.4.

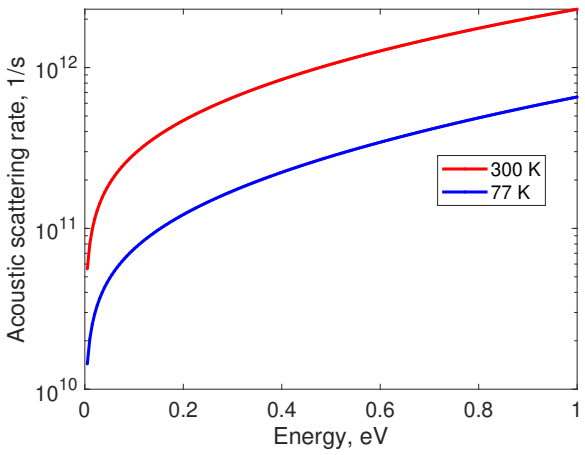

FIGURE 1.3: Total acoustic inelastic rate for GaAs at T=300 K and T=77 K.

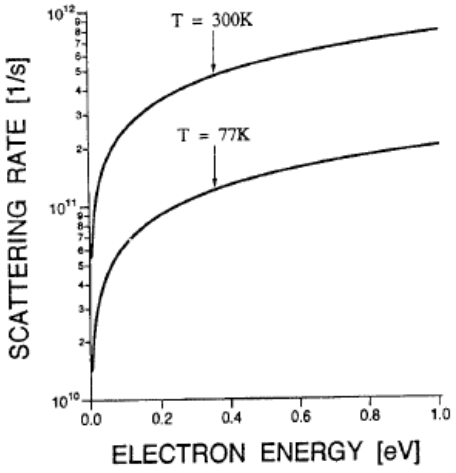

FIGURE 1.4: Literature data for total inelastic acoustic scattering rate [2].

As it can be seen, acoustic scattering rates strongly depends on temperature. Associated to an increasing temperature, the rate increases. This is due to the fact that ions' vibrational energy is higher with a higher number of associated phonons which can cause scattering. Moreover, higher is the energy of the initial state of the electron, higher the scattering rate will result. This is associated to the higher density of states for higher energies with respect to the bottom of the valley.

Elastic expression and comparison A simplified computation for this kind of scattering basically relies on the elastic equation (1.2).

$$W_{\text{aco}}(\mathbf{k}) = \frac{2\pi D_a^2 k_B T}{\hbar \nu_l^2 \rho} N(E_{\mathbf{k}}), \tag{1.2}$$

where $N(E_{\mathbf{k}})$ is the density of states associated to the studied valley (Γ in this case). It is worth noting that in the elastic case the absorption and emission spectra are equals. Moreover, in this approximation, the dependency of the energy on $\mathbf{k}$ just reduces on dependency on its modulus through the parabolic expression of energy $E_{\mathbf{k}} = \frac{\hbar^2 k^2}{2m^*}$. Comparison of this simulation with previous results is shown in Fig. 1.5 and 1.6 for both temperatures.
Clearly, the elastic expression provides always lower results with respect to the inelastic one. This behaviour is mainly linked to the parabolic approximation which gives less electronic states at higher energies if compared with the non parabolicity correction.

1.2 Intervalley (from Γ to L)

Scattering, furthermore, may cause an intervalley event assisted by non polar optical phonon (whose energy is $\hbar\omega_{ij}$). Here, simulation related to scattering from Γ valley to L one at 300 K is presented. In general, intervalley scattering assisted by non-polar optical phonon rate from valley i to valley j (with a valley energy difference $\Delta E_{ij} = 290\,\text{meV}$) is described by equation

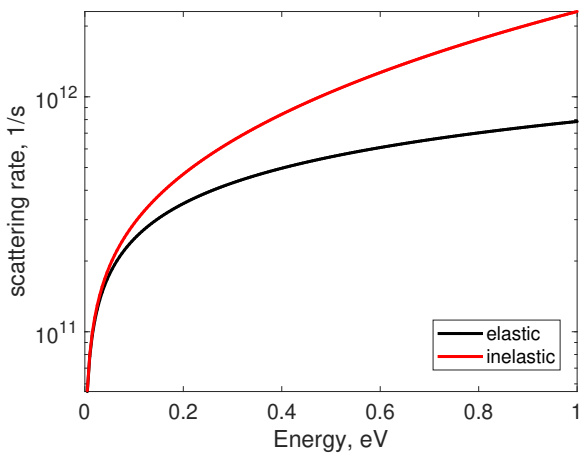

FIGURE 1.5: Inelastic and elastic acoustic scattering rates for GaAs at T=300 K.

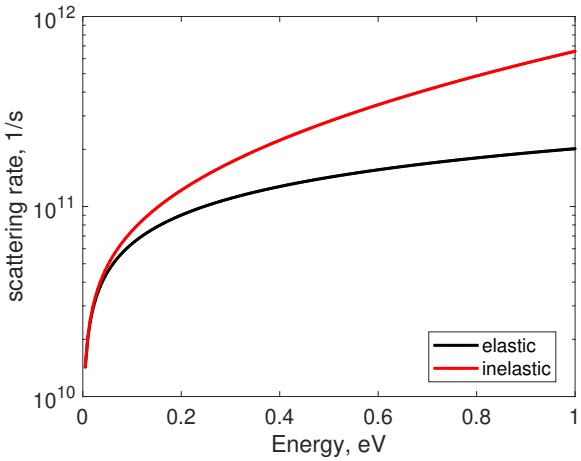

FIGURE 1.6: Inelastic and elastic acoustic scattering rates for GaAs at T=77 K.

(1.3).

$$W_{\text{iv}}(E) = \frac{\pi D_{ij}^2 Z_j}{\rho \omega_{ij}} \left(N_{ij} + \frac{1}{2} \mp \frac{1}{2} \right) N(E_{\mathbf{k}} \pm \hbar\omega_{ij} - \Delta E_{ji}), \tag{1.3}$$

where:

$$N_{ij} = \frac{1}{e^{\frac{\hbar\omega_{ij}}{k_B T}} - 1}, \tag{1.4}$$

is the number of intervalley phonons.
The plus and minus signs in equation (1.3) are related respectively to absorption and emission processes. During computation of parabolic density of states, due to non-isotropy of L-valley, the equivalent effective mass has been obtained as a weighted average along the three different directions:

$$m^* = (m_l m_t^2)^{1/3}. \tag{1.5}$$

The coefficient Z_j represents the number of equivalent final valleys. In the case of GaAs there are 8 equivalent valleys in the first Brillouin zone. However, each one is shared between to adjacent Brillouin zones giving as a result $Z_j = 4$. The physical constants have been obtained from [3, Chapter 11]. Moreover, the bottom of Γ valley is kept as reference for energies. Obtained results are compared with literature data [3, Chapter 2] and depicted in Fig. 1.7 and 1.8.
As it can be seen, both in the absorption and emission cases there is a threshold process. Threshold for the first one is linked to the fact that, in order to have non-zero values from density of states, it should hold $E_{\mathbf{k}} + \hbar\omega_{ij} \geq \Delta E_{ji}$. The second threshold arises from the condition $E_{\mathbf{k}} - \hbar\omega_{ij} \geq \Delta E_{ji}$. Again, the behaviour with respect to energy follows the density of states one.

1.3 Polar Scattering by Optical Phonons

The interaction of electrons with polar optical phonons is the dominant scattering mechanism in polar semiconductors as GaAs (III-V semiconductor) at room temperature and in equilibrium condition. The following results are based on the Fröhlich formulation and taking into account that only longitudinal optical modes generate a dipole field. The latter are described by means of a dispersionless relation and screening effects are neglected in the following. Furthermore, it is an anisotropic scattering mechanism, given the matrix element of the Fermi Golden Rule

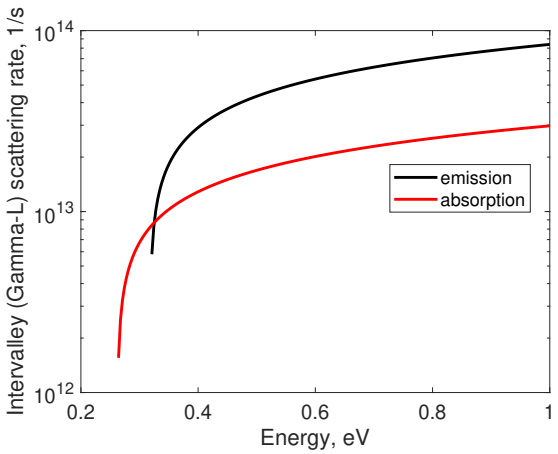

FIGURE 1.7: Simulated Γ to L intervalley scattering rates (emission and absorption) assisted by non polar optical phonon for GaAs.

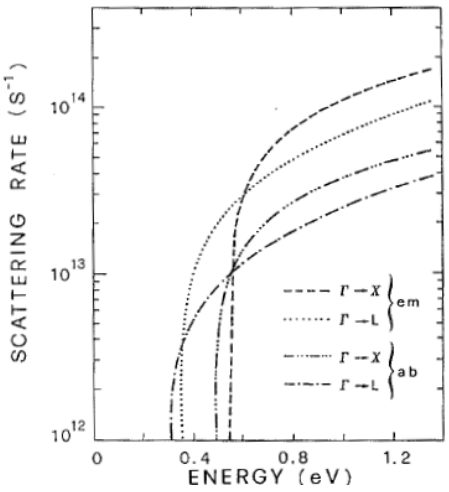

FIGURE 1.8: Literature data [3] for intervalley (Γ to L) scattering rates assisted by non polar optical phonon in GaAs.

being dependent on the inverse square of the phonon wavevector.

For a **parabolic band**, the scattering rate is given by

$$W_{\text{pop}}(\mathbf{k}) = \frac{e^2\omega_{\text{LO}}}{8\pi\epsilon_p}\frac{k}{E_{\mathbf{k}}}\left\{N_q + \frac{1}{2} \mp \frac{1}{2}\right\}\ln\left(\frac{q_{\max}}{q_{\min}}\right), \tag{1.6}$$

where the upper sign refers to an absorption process, $q_{\max} = k\left|1 + \sqrt{1 \pm \hbar\omega_{\text{LO}}/E_{\mathbf{k}}}\right|$ and $q_{\min} = k\left|1 - \sqrt{1 \pm \hbar\omega_{\text{LO}}/E_{\mathbf{k}}}\right|$. Finally, $\epsilon_p = 1/(1/\epsilon_\infty - 1/\epsilon_s)$, where the last two parameters are the dielectric constants at high and low frequency, respectively. The energy dependence of the scattering rate is shown in Fig. 1.9a for the Γ valley of GaAs at 300 K.

For a **nonparabolic band**, the scattering rate is given by

$$W_{\text{pop}} = \frac{e^2\sqrt{m^*}\omega_{\text{LO}}}{4\pi\epsilon_p\sqrt{2}\hbar\sqrt{\gamma(E_i)}}\frac{\partial\gamma(E_f)}{\partial E_f}\left\{N_q + \frac{1}{2} \mp \frac{1}{2}\right\}\frac{1}{\text{C}}\left\{\text{A}\ln\left|\frac{\gamma^{1/2}(E_i) + \gamma^{1/2}(E_f)}{\gamma^{1/2}(E_i) - \gamma^{1/2}(E_f)}\right| + \text{B}\right\}, \tag{1.7}$$

being A, B and C parameters dependent on the nonparabolic density of states and the electron kinetic energy before and after the scattering, found in the lecture notes [1]. The result is shown in Fig. 1.9b for the Γ valley of GaAs at 300 K.

From Fig. 1.9 it is evident that in both cases the scattering efficiency decreases with increasing energy. Nevertheless, in the parabolic valley approximation there is an overall decrease of the scattering rate $W_{\text{pop}} \propto 1/\sqrt{E_{\mathbf{k}}}$ for sufficiently high energy values. On the other hand, in the nonparabolic valley approximation the scattering rates decrease with lower pace because its density of states takes into account a much higher number of states with respect to the parabolic one.

Last, it is possible to appreciate the similarity between Fig. 1.9b and Fig. 1.10 taken from [4, Chapter 2], from which the physical constants are taken.

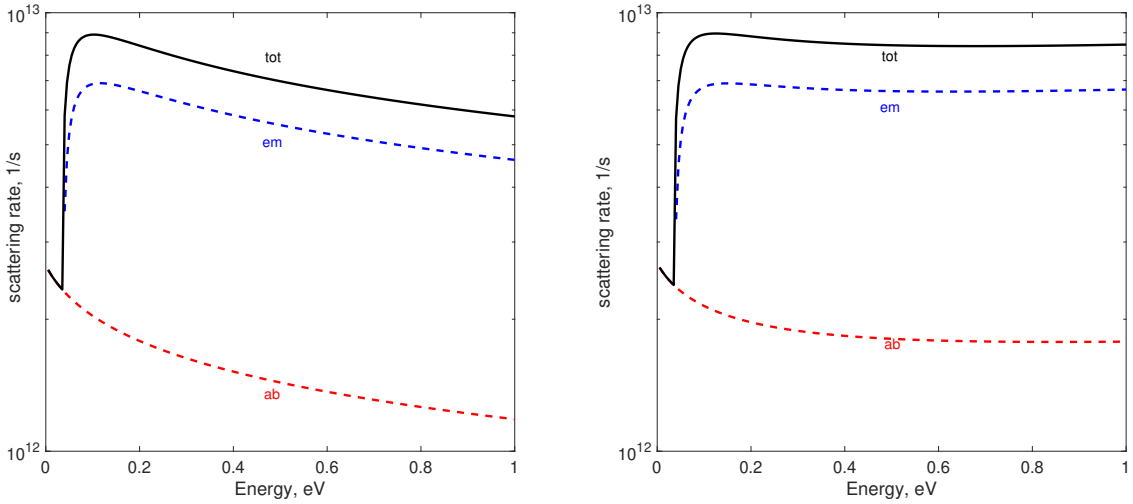

(A) (B)

FIGURE 1.9: Energy dependence of the polar optical scattering rate for the Γ valley of GaAs at 300 K, in the (A) parabolic and (B) nonparabolic valley approximation.

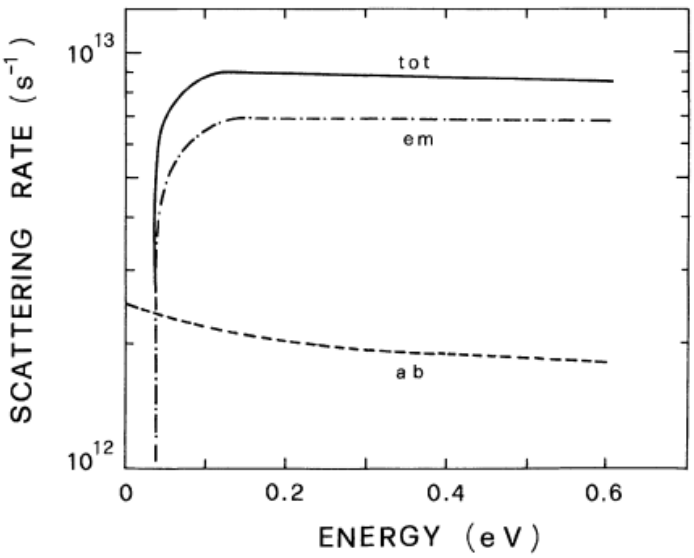

FIGURE 1.10: Energy dependence of the polar optical scattering rate for the Γ valley of GaAs at 300 K, in the nonparabolic valley approximation, from [4].

1.4 Ionized Impurity Scattering

This type of scattering is elastic and it is not sufficient to monitor the transport process in the presence of an external field. Therefore, it would require some dissipative scattering mechanism in order to obtain the correct electron energy in any simulation.
By considering the Brooks and Herring approach, an exponential screening factor is introduced and the Coulombic potential drops off more rapidly with respect to the expression with no screening. The screened potential becomes

$$\mathrm{V}(r) = \frac{Ze^2}{4\pi\epsilon_s r} e^{-q_0 r}, \tag{1.8}$$

where Z is the number of charge units of the impurity and the reciprocal length is given by

$$q_0 = \sqrt{\frac{e^2 n_0}{\epsilon_s k_B T}},$$

being n_0 the equilibrium electron density and ϵ_s the low frequency dielectric constant. Given the impurities concentration n_I, the scattering rate results to be

$$W_{\mathrm{imp}}^{(BH)}(\mathbf{k}) = \frac{\pi n_I Z^2 e^4 N(E_{\mathbf{k}})}{\hbar \epsilon_s^2} \frac{2}{q_0^2(4k^2 + q_0^2)}. \tag{1.9}$$

Fig. 1.11 shows the scattering rates calculated for $n_I = 1 \times 10^{16}\,\mathrm{cm}^{-3}$ and $n_I = 1 \times 10^{18}\,\mathrm{cm}^{-3}$, $Z = 1$ in the nonparabolic approximation. The `Matlab` script correctly describes the lower scattering rate as the impurity concentration increases, which is clear in the low energy region. The reason stands in equation (1.9), since for small $|\mathbf{k}|$ values the denominator is nearly proportional to $n_0^2 \approx n_I^2$, whilst the numerator is proportional to n_I. However, the mobility will decrease by increasing the impurity concentration due to the greater screening.

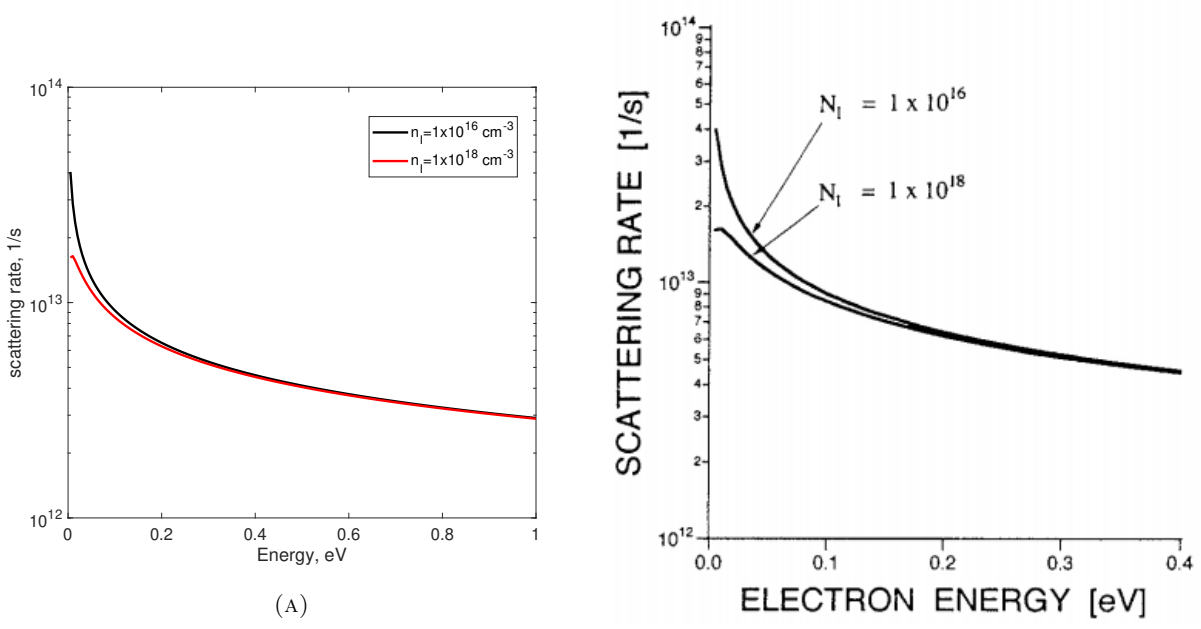

(A) (B)

FIGURE 1.11: Scattering rate of the ionized impurities in GaAs at $T = 300\,\mathrm{K}$ when $n_0 = n_I$ and Z=I, (A) from equation (1.9) (B) from [2, Chapter 2].

Chapter 2

Solving the Boltzmann Equation

2.1 Mobility of GaAs in the Relaxation Time Approximation

The aim of this section is to evaluate the low-field mobility of GaAs due to impurity and deformation potential acoustic scattering as a function of temperature according to Matthiessen's rule $\mu_0^{-1} = \mu_{\text{aco}}^{-1} + \mu_{\text{imp}}^{-1}$.
By taking into account that **acoustic scattering** is velocity randomizing, the momentum relaxation time coincides with the inverse scattering rate in the case of nondegenerate statics. Moreover, the elastic approximation (1.2) has been considered. It results

$$\frac{1}{\tau_{\text{aco}}(E_{\mathbf{k}})} = W_{\text{aco}}(E_{\mathbf{k}}). \tag{2.1}$$

Being **impurity scattering** an elastic process, it is found that

$$\begin{aligned}\frac{1}{\tau_{\text{imp}}^{(\text{BH})}(E_{\mathbf{k}})} &= \frac{\pi n_I Z^2 e^4 N(E_{\mathbf{k}})}{\hbar \epsilon_s^2} \int_{-1}^{1} \frac{(1-\cos\theta)\mathrm{d}(\cos\theta)}{\left[2k^2\,(1-\cos\theta)+q_0^2\right]^2} = \\ &= \frac{\pi n_I Z^2 e^4 N(E_{\mathbf{k}})}{\hbar \epsilon_s^2} \frac{1}{4k^4}\left[\log\left(1+\frac{4k^2}{q_0^2}\right)-1\right],\end{aligned} \tag{2.2}$$

where the last integral has been computed by exploiting `Matlab` Symbolic Toolbox.
The mobilities are evaluated by spanning over the energy space

$$\mu_0 = \frac{e}{m^*}\frac{2}{3k_B T}\frac{\int \mathrm{d}E f_M(E) E\,\tau(E) N(E)}{\int \mathrm{d}E f_M(E) N(E)}, \tag{2.3}$$

being f_M the Maxwell-Boltzmann approximation of the Fermi-Dirac distribution function in the nondegenerate limit [1]. The results are shown in Fig. 2.1a. For high temperatures it is clear from Fig. 2.1b that polar optical scattering is the predominant scattering mechanism in GaAs at ambient temperatures. Being neither velocity randomizing nor elastic, it cannot be modelled within the relaxation time approximation. However, at lower temperatures, deformation potential scattering of acoustic phonons becomes more important with respect to the optical one. Ultimately, ionized impurity scattering is the most effective process at very low temperatures, around 20 K. The mobility associated to acoustic photons is the same in both plots of Fig. 2.1, yet the impurity one is not. Indeed, the computed μ_{imp} values are smaller by one order of magnitude with respect to Fig. 2.1b. To investigate the mismatch, equation (2.3) and the book equation [3, Equation 11.49] have been plotted in Fig. 2.2. They are superimposed except at low temperatures, due the approximation embedded in [3, Equation 11.49].

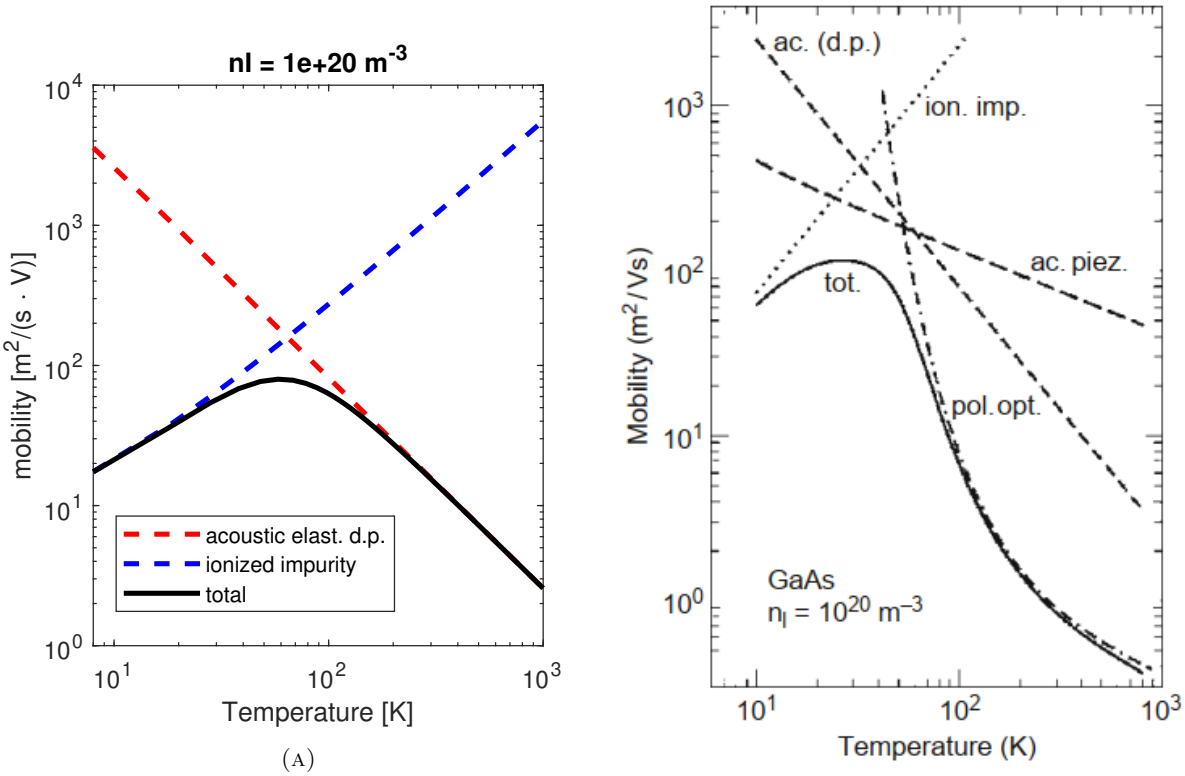

(A) (B)

FIGURE 2.1: Electron mobilities in GaAs combined with Matthiessen rule, (A) from equation (2.3) (B) from [3, Chapter 11]

.

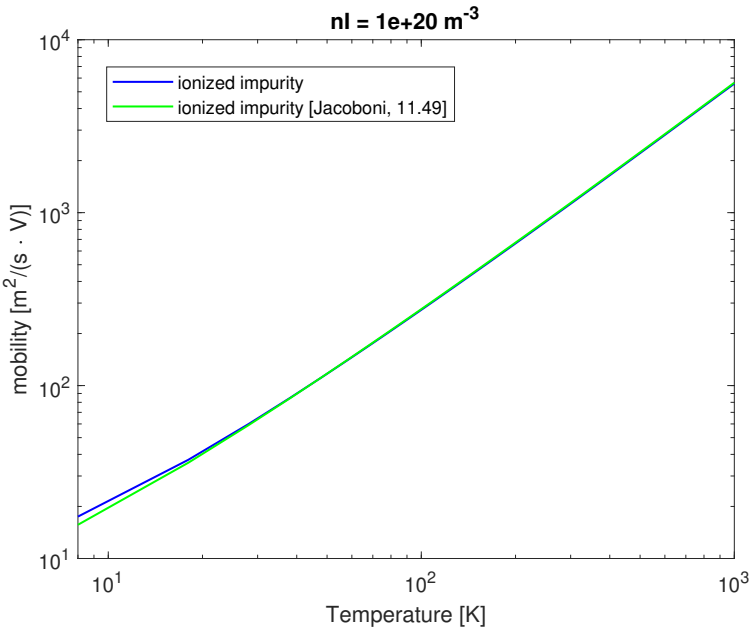

FIGURE 2.2: Mobilities from ionized impurity $n_I = 1 \times 10^{14}\,\mathrm{cm}^{-3}$ in GaAs, (A) from equation (2.3) (B) from [3, Equation 11.49].

2.2 Monte Carlo Simulation of Bulk Properties of GaAs

In the following the results obtained by *single particle* Monte Carlo simulations are presented. The model comprehends the two Γ and L valleys in the non parabolic effective mass approximation. Indeed, the anisotropy of the L-valleys is not taken into account and they are modelled as four equivalent spherical bands. The associated density of states is m_d^* according to Eq. (1.5). The algorithm is based on [1] and the flow-chart is shown in Fig. 2.3. The scripts of Chapter 1 have been readily converted into functions and they have been slightly modified to take into account the two different valleys. Within the semi classical approach, the driving force is an electric field along the x-axis, whose choice is based on the rotation matrix [2] addressed afterwards.
Actually, two versions of the Monte Carlo code have been developed. In the first one the scattering rates are evaluated at the end of each drift step, whereas in the second case they have been tabulated by sampling over an energy interval. No appreciable effects have been obtained between the two implementations. Unless otherwise stated, the tabulated one has been used to plot all the physical quantities. The reason lies in the lower computational cost.

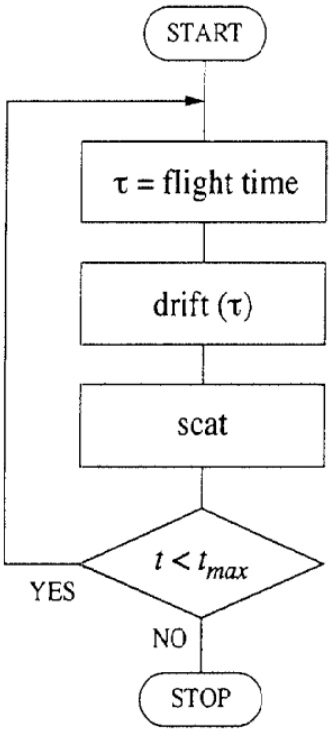

FIGURE 2.3: Flowchart of a single particle Monte Carlo simulation. Reproduced from [2, Chapter 3].

The scattering mechanism is chosen by the *inversion technique* [1] by means of pseudorandom numbers. If no scattering occurs, the electron remains in its original state. The plot of

$$\tau\Lambda_n(E_{\mathbf{k}}) = \tau \sum_{j=1}^{n} W_j(E_{\mathbf{k}}), \quad \text{flight time } \tau = 0.1\,\text{fs} \ll 1/W_{\text{T}}(E_{\mathbf{k}})$$

is shown in Fig. 2.4 for the Γ- valley, whose index is iv = 1. The new state after scattering is chosen randomly by working in a new reference system with $\mathbf{k}'_{\mathbf{z}}$ parallel to the electron wavevector before scattering. At the end, a rotation matrix [2] is applied to retain the new components in

the *laboratory frame*. It is recalled that acoustic piezoeletric scattering has not been implemented and intervalley scattering has been limited to $\Gamma \leftrightarrow$ L valleys, excluding L $\leftrightarrow$ L, $\Gamma \leftrightarrow$ X transitions. Deformation potential scattering is treated in the elastic approximation.

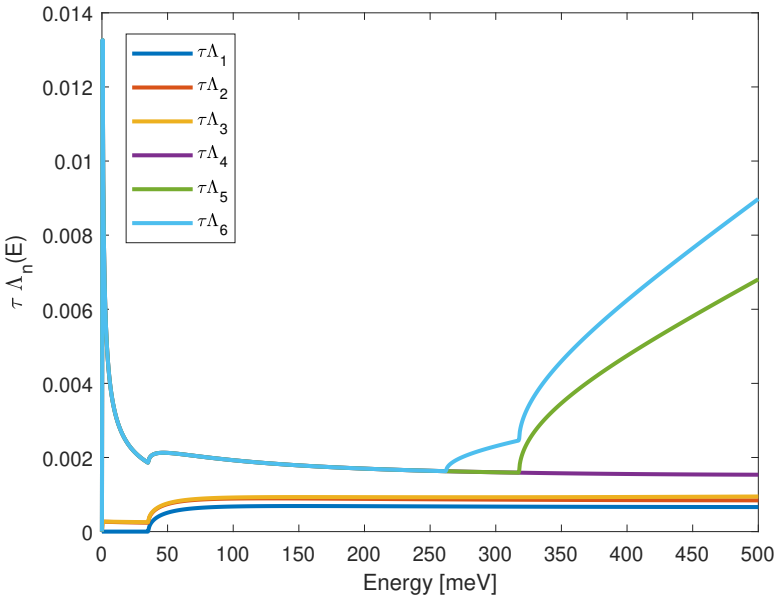

FIGURE 2.4: Plot of $\tau\,\Lambda_n(E_{\mathbf{k}})$ in Γ-valley for the tabulated Monte Carlo.

2.2.1 Average Electron Velocity, Energy and Occupancy

In Fig. 2.5 it is shown the $v - F$ curve for electrons in bulk GaAs at the temperature of 300 K. For each electric field, the standard deviation has been computed by considering the last 90% mean velocities in the overall simulation $\tau_{sim} = 1$ ns. In Fig. 2.5a the decrease of the electron velocity occurs at the threshold value of approximately 6 kV cm^{-1}, which is slightly greater than the literature (2.5b) one of about 4 kV cm^{-1}. Nevertheless, the so called *negative differential conductivity* well resembles the drop of $\sim 1\times10^7$ cm s^{-1} between the peak value and the saturated one at 50 kV cm^{-1}.

Fig. 2.6 shows the **electron mean kinetic energy** as a function of the electric field. The standard deviation has been evaluated as before. Notice that for low fields the electron energy is close to $1.5\,k_B\,T \approx 39$ meV. It can be appreciated that the electron energy increases rapidly as the electron field is lower than the threshold field for NDM. Indeed, as the fields becomes sufficiently high, the energy gained by the electrons during each single flight is not negligible. Intravalley optical-phonon scattering is not able to dissipate the electron energy. Afterwards, the energy increment is slower because electron occupancy in L-valley increases. This results in higher energy relaxation rate due to intervalley scattering. The latter is very effective in dissipating both energy and momentum, and the velocity decreases giving rise to the NDM phenomenon. The main difference is the average electron energy for higher electric fields, being in Fig. 2.6a smaller than Fig. 2.6b by about 36%.

In the preceding paragraph it has been stated that as the electric fields gets stronger, the electron spends in average more time in the L valley. This is clearly shown in Fig. 2.7a. Close to 15 kV cm^{-1} the **occupancy probabilities** of the two valleys cross each other until the L-valley occupancy saturates at about 80%. The population inversion occurs for slightly lower fields according to [2].

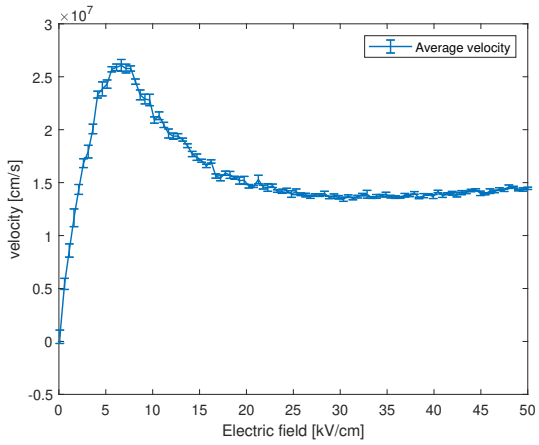

(A)

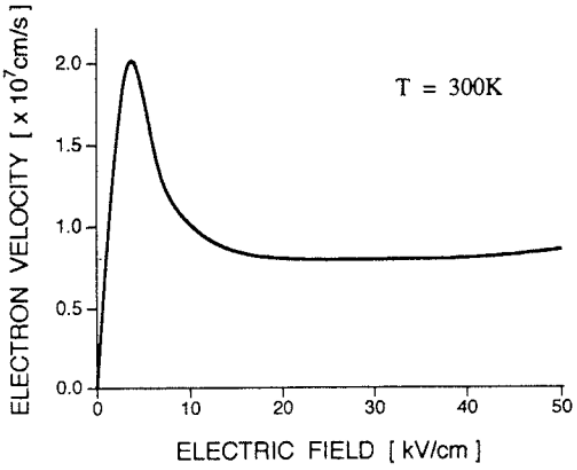

(B)

FIGURE 2.5: Electron velocity versus electric field curve calculated for bulk GaAs at 300 K (A) tabulated MC (B) literature [2]. The ionized impurity concentration is $1 \times 10^{14}\,\mathrm{cm}^{-3}$.

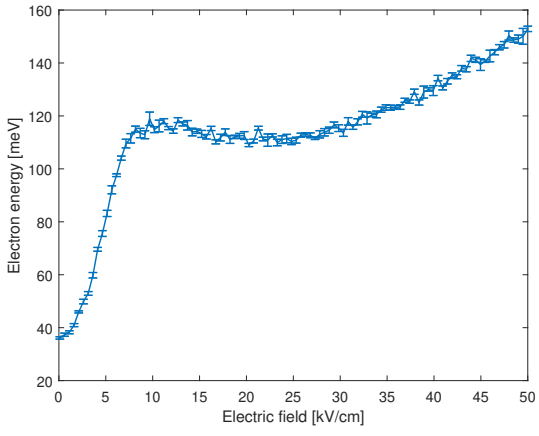

(A)

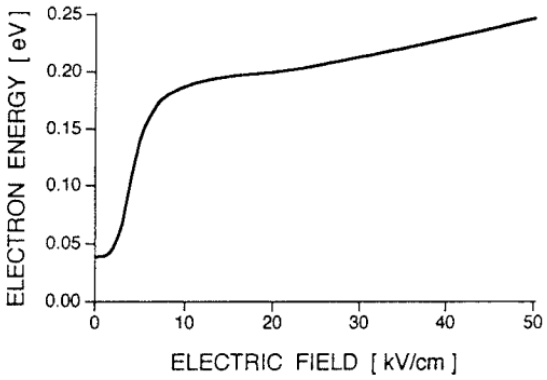

(B)

FIGURE 2.6: Mean electron kinetic energy versus electric field curve calculated for bulk GaAs at 300 K (A) tabulated MC (B) from [2]. The ionized impurity concentration is assumed to be $1 \times 10^{14}\,\mathrm{cm}^{-3}$.

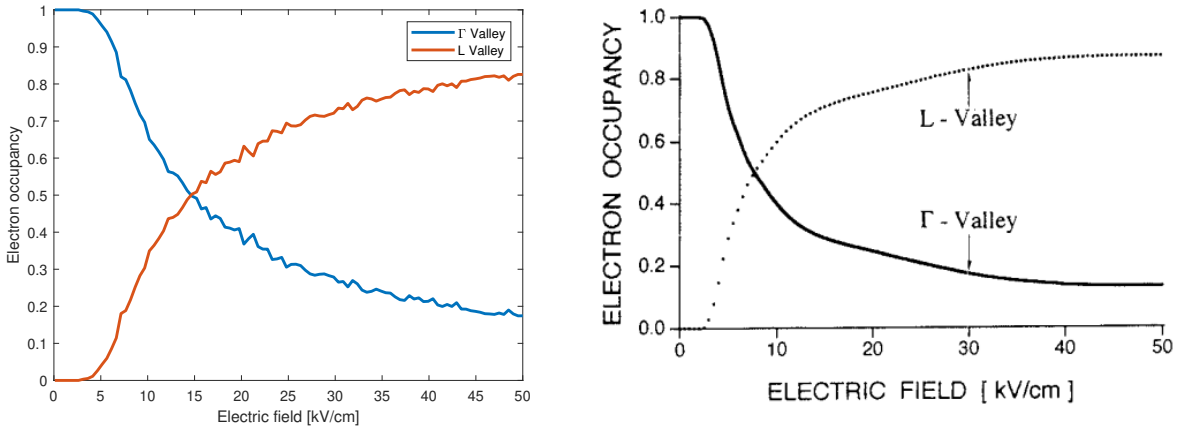

(A) (B)

FIGURE 2.7: Electron occupancy in the Γ− and L− valleys versus electric field curve calculated for bulk GaAs at 300 K (A) tabulated MC (B) from [2]. The ionized impurity concentration is $1 \times 10^{14}\,\mathrm{cm}^{-3}$.

2.2.2 Noise Diffusivity

In the following, the longitudinal diffusivity in GaAs as function of electric field is computed. The choice of the longitudinal component along the field is to remove the tensorial description of the process, simplifying the computation. Since the diffusion is a process which relies on noise, its description starts from the autocorrelation function of velocity fluctuations

$$C_v(\tau) = \langle \delta v(t) \delta v(t+\tau) \rangle \,, \tag{2.4}$$

where the fluctuations are computed with respect to the mean velocity

$$\delta v(t) = v(t) - \langle v(t) \rangle \,. \tag{2.5}$$

The diffusivity is obtained by integrating eq. (2.4)

$$D = \int_0^\infty C_v(\tau) d\tau. \tag{2.6}$$

Physically, it means that longer is the persistence of velocity fluctuations, higher will the diffusivity be.
Two autocorrelation functions are shown in figures 2.8a and 2.8b respectively for low and high field. The former, as expected from theory, exhibits a monotonic exponential decreasing up to zero. The latter, on the contrary, reaches negative values and then converges to zero too, but from the negative side. This negative tail is related to the competing effects of momentum relaxation and energy relaxation. Concerning diffusivity, the result is shown in figure 2.9a and compared to literature data [5] in figure 2.9b.

As it can be seen, the diffusivity rapidly decrease for fields around $10\,\mathrm{kV\,cm}^{-1}$, and reaches a saturation value corresponding to about $1.2\,\mathrm{cm}^2\,\mathrm{s}^{-1}$ for very high fields, in agreement with literature. This behaviour is linked to the different occupation of valleys for high fields as shown in fig. 2.7: when the L-valley is more populated, the mobility and diffusivity are lower than the equilibrium condition.

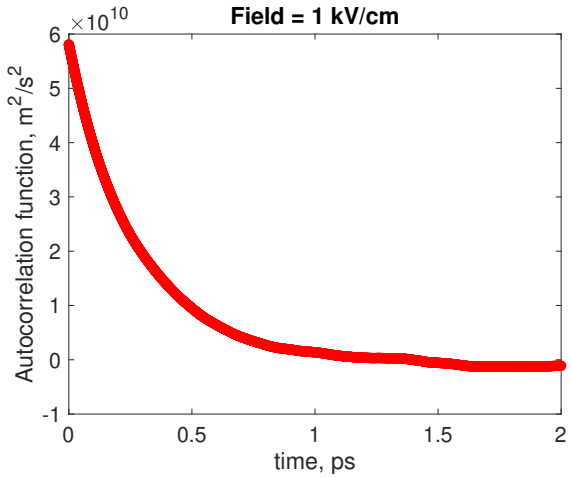

(A) Autocorrelation function for an electric field of $1\,\mathrm{kV\,cm^{-1}}$ (low field).

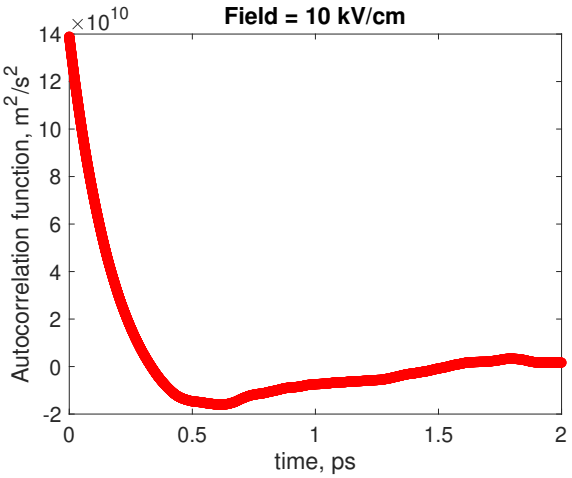

(B) Autocorrelation function for an electric field of $10\,\mathrm{kV\,cm^{-1}}$ (high field).

FIGURE 2.8

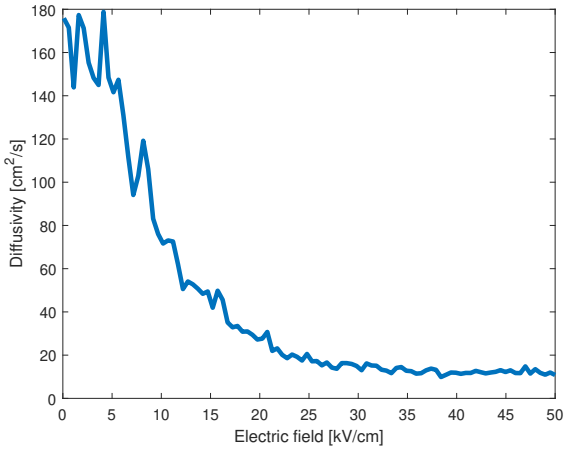

(A) Simulated diffusion coefficient as function of electric field for GaAs at T=300 K.

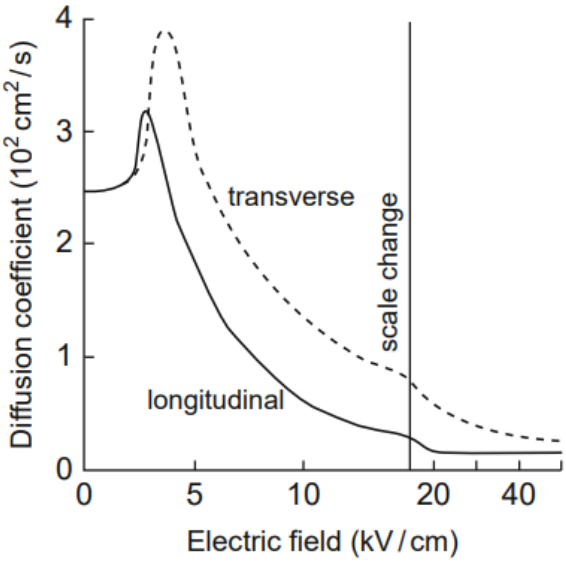

(B) Literature diffusion coefficient as function of electric field for GaAs at T=300 K [5].

FIGURE 2.9

Diffusivity and mobility are strictly related by Einstein relation:

$$D = \frac{k_B T}{q} \mu, \tag{2.7}$$

which is valid only under equilibrium condition. In figure 2.10 three different results for mobility are compared: the one from Montecarlo simulation through the ratio between velocity and field, the one with the relaxation time approach and the one obtained from eq. (2.7). It is worth observing that the second mentioned is constant since it has been computed only for equilibrium condition. Moreover, the relaxation time mobility is significantly higher than the others since the former includes only acoustic and impurity scattering. Even if Einstein relation is valid only in equilibrium condition, it has been extended for electric fields different from zero too, showing a still valid approximation for the mobility behaviour out of equilibrium.

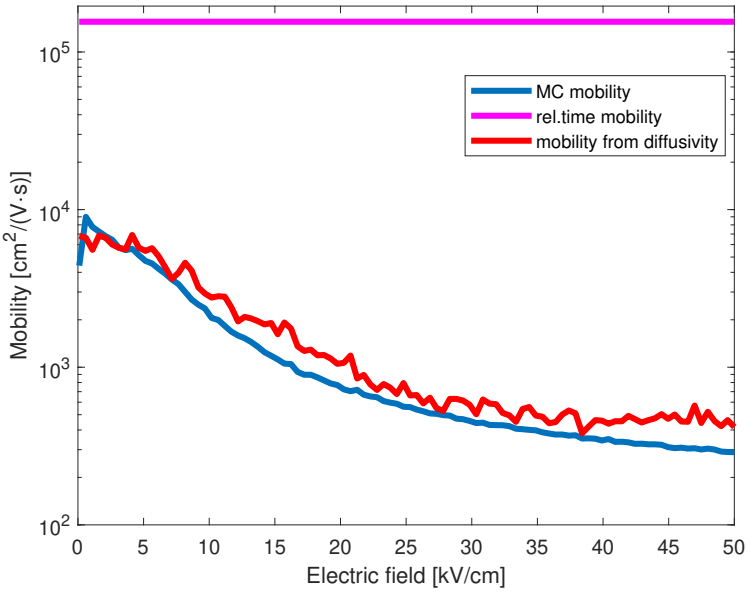

FIGURE 2.10: Comparison between Montecarlo simulation mobility, relaxation time mobility (only under equilibrium) and mobility from diffusivity through Einstein relation.

2.2.3 Impact ionization coefficient

As a final task, the impact ionization coefficient for bulk GaAs electrons has been computed as a function of the electric field. Including the additional impact ionization scattering rate in the Montecarlo simulation through the Keldysh formula

$$W_{ii}(E) = \frac{P}{\tau_{ep}(E_{th})} \left(\frac{E - E_{th}}{E_{th}} \right)^2, \tag{2.8}$$

the mean free path between each one of these events has been computed. Averaging it and taking the reciprocal value, the ionization coefficient has been obtained. Results are shown in figure 2.11a and compared to literature data [5] in figure 2.11b. Obviously the ionization coefficient increases as the field gets stronger, since electrons are more energetic and the probability of an impact event is higher.

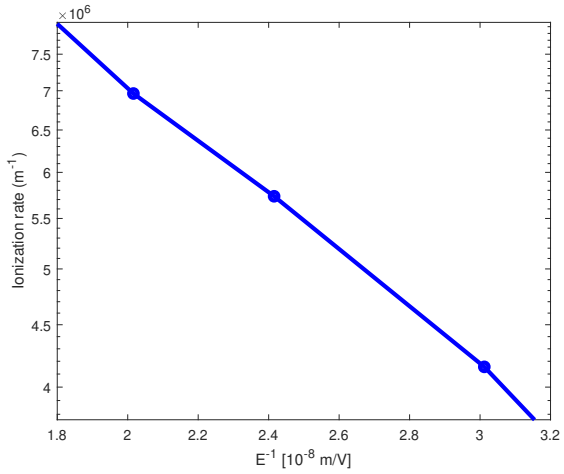

(A) Simulated impact ionization coefficient for electrons as function of reciprocal electric field for GaAs at T=300 K.

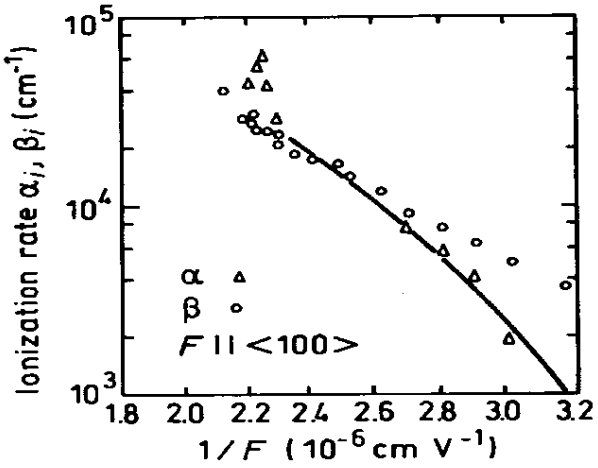

(B) Literature impact ionization coefficient as function of reciprocal electric field for GaAs at T=300 K [5]. α and β are ionization coefficients for electrons and holes respectively.

FIGURE 2.11

2.3 Conclusions

In the first chapter, different scattering rates have been evaluated and compared with literature values, obtaining much similar results. In the second part, the mobility has been obtained by means of the relaxation time approximation for deformation potential and ionized impurity scattering, obtaining results in good agreement with [3], given the correction for the ionized impurities dependent mobility discussed in the corresponding section.
Last, it has been shown that a simple analytical band structure for GaAs in the effective mass approximation is able to reproduce transport phenomena by a single particle Monte Carlo simulation. Numerical values differing from [2] are attributed to the absence of $\mathrm{L} \leftrightarrow \mathrm{L}, \Gamma \leftrightarrow \mathrm{X}$ transitions. In addition, the bulk impact ionization process has been simulated using a Keldysh scattering probability, obtaining the same order of magnitude for higher fields with respect to literature data.

Appendix A

Scattering rates - MATLAB code

A.1 Acoustic deformation potential scattering

```
clear all
close all

% constants
c_light = 2.99792458e+8; % light velocity, m/s
H = 6.626070040e-34; % Planck constant, J*s
HBAR = 1.054D-34; % reduced Planck constant, J*s
kB = 1.3806488e-23; % Boltzmann constant, J/K
Q = 1.6021766208e-19; % elementary charge, C
%T = 300; % temperature, K
eps0 = 8.854D-12; % vacuum permittivity constant, F/m
M0 = 9.1095D-31; % electron mass, kg
rho = 5320; % mass density, kg/m^3
eps_s = 12.9*eps0; % static dielectric constant, F/m
eps_infty = 10.9*eps0; % high-frequency dielectric constant, F/m
v_l = 5240; % longitudinal sound velocity, m/s
meff = 0.067*M0; % effective mass, kg
alpha = 0.64/Q; % nonparabolicity factor, 1/J
hwpop = 0.0354*Q; % longitudinal optical phonon energy, J
Daco = 7*Q; % acoustic deformation potential, J
egap = 1.424*Q; % energy gap, J
%%
nE = 200; % number of energy points
vE = linspace(0,1,nE)*Q; % energy axis, J
Waco_abs_300 = zeros(1,nE);
Waco_emi_300 = zeros(1,nE);
Waco_abs_77 = zeros(1,nE);
Waco_emi_77 = zeros(1,nE);
T=[300 77];
for ie = 1:nE,
E = vE(ie);
[Waco_emi_300(ie), Waco_abs_300(ie)] = aco_scat_inelastic(E,T(1));
[Waco_emi_77(ie), Waco_abs_77(ie)] = aco_scat_inelastic(E,T(2));
end

figure(1), hold on
semilogy(vE/Q,Waco_emi_300,'r.-','linewidth',2)
semilogy(vE/Q,Waco_abs_300,'b.-','linewidth',2)
```

```
semilogy(vE/Q,Waco_emi_300+Waco_abs_300,'k.-','linewidth',2)
set(gca,'FontSize',14,'FontName','Arial','box','on')
ylabel('Acoustic scattering rate (300 K), 1/s'), xlabel('Energy, eV')
legend('emission','absorption','total')

figure(2), hold on
semilogy(vE/Q,Waco_emi_77,'r.-','linewidth',2)
semilogy(vE/Q,Waco_abs_77,'b.-','linewidth',2)
semilogy(vE/Q,Waco_emi_77+Waco_abs_77,'k.-','linewidth',2)
set(gca,'FontSize',14,'FontName','Arial','box','on')
ylabel('Acoustic scattering rate, 1/s (77 K)'), xlabel('Energy, eV')
legend('emission','absorption','total')

figure(3), hold on
semilogy(vE/Q,Waco_emi_300+Waco_abs_300,'r.-','linewidth',2)
semilogy(vE/Q,Waco_emi_77+Waco_abs_77,'b.-','linewidth',2)
set(gca,'FontSize',14,'FontName','Arial','box','on')
ylabel('Acoustic scattering rate, 1/s'), xlabel('Energy, eV')
legend('300 K','77 K')

%% elastic approximation (emission rate = absorption rate)
N=@(E) ((2*meff)^(1.5))*sqrt(E)/(4*pi^(2)*HBAR^(3));

nE = 200; % number of energy points
vE = linspace(0,1,nE)*Q; % energy axis, J
for ie = 1:nE,
E = vE(ie);
Waco_elastic_300(ie)=(2*pi*Daco^(2)*kB*T(1))/(HBAR*v_l^(2)*rho)*N(E);
Waco_elastic_77(ie)=(2*pi*Daco^(2)*kB*T(2))/(HBAR*v_l^(2)*rho)*N(E);
end

figure(4), hold on
semilogy(vE/Q,Waco_elastic_300,'k.-','linewidth',2)
semilogy(vE/Q,Waco_emi_300+Waco_abs_300,'r.-','linewidth',2)
set(gca,'FontSize',14,'FontName','Arial','box','on')
ylabel('Acoustic scattering rate, 1/s'), xlabel('Energy, eV')
legend('elastic','inelastic')
title('300 K')

figure(5), hold on
semilogy(vE/Q,Waco_elastic_77,'k.-','linewidth',2)
semilogy(vE/Q,Waco_emi_77+Waco_abs_77,'r.-','linewidth',2)
set(gca,'FontSize',14,'FontName','Arial','box','on')
ylabel('Acoustic elastic scattering rate, 1/s'), xlabel('Energy, eV')
legend('elastic','inelastic')
title('77 K')
```

A.2 Intervalley scattering from Γ to L

```
clear all
```

```
close all

% constants
c_light = 2.99792458e+8; % light velocity, m/s
H = 6.626070040e-34; % Planck constant, J*s
HBAR = 1.054D-34; % reduced Planck constant, J*s
kB = 1.3806488e-23; % Boltzmann constant, J/K
Q = 1.6021766208e-19; % elementary charge, C
T = 300; % temperature, K
eps0 = 8.854D-12; % vacuum permittivity constant, F/m
M0 = 9.1095D-31; % electron mass, kg
rho = 5320; % mass density, kg/m^3
eps_s = 12.9*eps0; % static dielectric constant, F/m
eps_infty = 10.9*eps0; % high-frequency dielectric constant, F/m
v_l = 5240; % longitudinal sound velocity, m/s
meff = 0.067*M0; % effective mass, kg
alpha = 0.64/Q; % nonparabolicity factor, 1/J
hwpop = 0.0354*Q; % longitudinal optical phonon energy, J
Daco = 7*Q; % acoustic deformation potential, J
egap = 1.424*Q; % energy gap, J
Dij=1e+11*Q; %coupling constant gamma-L [J/m]
meff_ij=(1.2*0.2^2)^(1/3)*M0;
deltaE_ij=0.29*Q; % delta energy gamma-L valleys, J
omega_ij=0.0278*Q/HBAR; % da libro HESS pag.108
Nij=1/(exp((HBAR*omega_ij)/(kB*T))-1);
%%
coeff=(pi*Dij^(2)*4)/(rho*omega_ij);
N=@(E) ((2*meff_ij)^(1.5))*sqrt(E)/(4*pi^(2)*HBAR^(3));

nE = 300; % number of energy points
vE = linspace(0,1,nE)*Q; % energy axis, J
W_gamma_L_emi=zeros(1,200);
W_gamma_L_abs=zeros(1,200);
for ie = 1:nE,
E = vE(ie);
if (E-HBAR*omega_ij-deltaE_ij>=0)
W_gamma_L_emi(ie)=coeff*N(E-HBAR*omega_ij-deltaE_ij)*(Nij+1);
end
if (E+HBAR*omega_ij-deltaE_ij>=0)
W_gamma_L_abs(ie)=coeff*N(E+HBAR*omega_ij-deltaE_ij)*(Nij);
end
end


plot(vE/Q, W_gamma_L_emi,'k','linewidth',2)
hold on
plot(vE/Q,W_gamma_L_abs,'r','linewidth',2)
set(gca,'FontSize',14,'FontName','Arial','box','on')
ylabel('Intervalley (Gamma-L) scattering rate, 1/s'), xlabel('Energy, eV')
legend('emission','absorption')
```

A.3 Polar Scattering by Optical Phonons

```
% constants
H = 6.626070040e-34; % Planck constant, J*s
HBAR = 1.054D-34; % reduced Planck constant, J*s
kB = 1.3806488e-23; % Boltzmann constant, J/K
Q = 1.6021766208e-19; % elementary charge, C
T = 300; % temperature, K
eps0 = 8.854D-12; % vacuum permittivity constant, F/m
M0 = 9.1095D-31; % electron mass, kg
eps_s = 12.9*eps0; % static dielectric constant, F/m
eps_infty = 10.9*eps0; % high-frequency dielectric constant, F/m
meff = 0.067*M0; % effective mass, kg
alpha = 0.64/Q; % nonparabolicity factor, 1/J
hwpop = 0.0354*Q; % longitudinal optical phonon energy, J
wpop=hwpop/HBAR;
egap = 1.424*Q; % energy gap, J
eps_p=1/(1/eps_infty-1/eps_s);
%%
gamma=@(E) E*(1+alpha*E); %for non parabolic
d_gamma=@(E) 1+2*alpha*E; %derivative of gamma(E)

A_e=@(E) (2*(1+alpha*E)*(1+alpha*(E-hwpop))+alpha*(gamma(E)+gamma(E-hwpop)))^2;
A_a=@(E) (2*(1+alpha*E)*(1+alpha*(E+hwpop))+alpha*(gamma(E)+gamma(E+hwpop)))^2;
B_e=@(E) -2*alpha*gamma(E)^(0.5)*gamma(E-hwpop)^(0.5)*(4*(1+alpha*E)...
*(1+alpha*(E-hwpop))+alpha*(gamma(E)+gamma(E-hwpop)));
B_a=@(E) -2*alpha*gamma(E)^(0.5)*gamma(E+hwpop)^(0.5)*(4*(1+alpha*E)...
*(1+alpha*(E+hwpop))+alpha*(gamma(E)+gamma(E+hwpop)));
C_e=@(E) 4*(1+2*alpha*E)*(1+2*alpha*(E-hwpop))*(1+alpha*E)*(1+alpha*(E-hwpop));
C_a=@(E) 4*(1+2*alpha*E)*(1+2*alpha*(E+hwpop))*(1+alpha*E)*(1+alpha*(E+hwpop));

k=@(E) sqrt(2*meff*E)/HBAR; %FOR PARABOLIC
qmin_abs=@(E) k(E)*abs(1-sqrt(1+hwpop/E));
qmin_emi=@(E) k(E)*abs(1-sqrt(1-hwpop/E));
qmax_abs=@(E) k(E)*abs(1+sqrt(1+hwpop/E));
qmax_emi=@(E) k(E)*abs(1+sqrt(1-hwpop/E));

coeff1=(Q^2*sqrt(meff)*wpop)/(4*pi*eps_p*sqrt(2)*HBAR);
coeff2=(Q^2*wpop)/(8*pi*eps_p);
B=bernoulli(sym(1:10));
z=sym('z','real');
x=sym('x','real');
nphon=1/z-1/2;
for m=1:5
nphon = nphon + B(2*m)*z^(2*m-1)/factorial(2*m);
end
z=(hwpop)/(kB*T);
Nq=double(subs(nphon)); %well approximates the exact form (line below)
%Nq=1/(exp((hwpop)/(kB*T))-1);

nE = 200; % number of energy points
```

```
vE = linspace(0,1,nE)*Q; % energy axis, J
Wpop_inelastic_abs=zeros(1,nE);
Wpop_inelastic_emi=zeros(1,nE);
Wpop_parabolic_abs=zeros(1,nE);
Wpop_parabolic_emi=zeros(1,nE);
for ie = 1:nE
E = vE(ie);
Wpop_inelastic_abs(ie)=(coeff1/sqrt(gamma(E)))*d_gamma(E+hwpop)*(Nq)*...
(1/C_a(E))*(A_a(E)*log(abs((gamma(E)^(0.5)+gamma(E+hwpop)^(0.5))/(gamma(E)^(0.5)...
-gamma(E+hwpop)^(0.5))))+B_a(E));
Wpop_parabolic_abs(ie)=(coeff2*(k(E)/E))*(Nq)*log(qmax_abs(E)/qmin_abs(E));
if (E>=hwpop)
Wpop_inelastic_emi(ie)=(coeff1/sqrt(gamma(E)))*d_gamma(E-hwpop)*(Nq+1)*...
(1/C_e(E))*(A_e(E)*log(abs((gamma(E)^(0.5)+gamma(E-hwpop)^(0.5))/(gamma(E)^(0.5)...
-gamma(E-hwpop)^(0.5))))+B_e(E));
Wpop_parabolic_emi(ie)=(coeff2*(k(E)/E))*(Nq+1)*log(qmax_emi(E)/qmin_emi(E));
end
end

figure(1)
plot(vE/Q, Wpop_inelastic_emi,'b','linewidth',2)
hold on
plot(vE/Q,Wpop_inelastic_abs,'r','linewidth',2)
plot(vE/Q,Wpop_inelastic_abs+Wpop_inelastic_emi,'k','linewidth',2)
set(gca,'FontSize',14,'FontName','Arial','box','on')
ylabel('Polar scattering rate (non parabolic), 1/s'), xlabel('Energy, eV')
legend('emission','absorption','total')

figure(2)
plot(vE/Q, Wpop_parabolic_emi,'b','linewidth',2)
hold on
plot(vE/Q,Wpop_parabolic_abs,'r','linewidth',2)
plot(vE/Q,Wpop_parabolic_abs+ Wpop_parabolic_emi,'k','linewidth',2)
set(gca,'FontSize',14,'FontName','Arial','box','on')
ylabel('Polar scattering rate (parabolic), 1/s'), xlabel('Energy, eV')
legend('emission','absorption','total')
```

A.4 Ionized Impurity scattering

```
% constants
c_light = 2.99792458e+8; % light velocity, m/s
H = 6.626070040e-34; % Planck constant, J*s
HBAR = 1.054D-34; % reduced Planck constant, J*s
kB = 1.3806488e-23; % Boltzmann constant, J/K
Q = 1.6021766208e-19; % elementary charge, C
T = 300; % temperature, K
eps0 = 8.854D-12; % vacuum permittivity constant, F/m
M0 = 9.1095D-31; % electron mass, kg
rho = 5320; % mass density, kg/m^3
eps_s = 12.9*eps0; % static dielectric constant, F/m
```

```
eps_infty = 10.9*eps0; % high-frequency dielectric constant, F/m
v_l = 5240; % longitudinal sound velocity, m/s
meff = 0.067*M0; % effective mass, kg
alpha = 0.64/Q; % nonparabolicity factor, 1/J
hwpop = 0.0354*Q; % longitudinal optical phonon energy, J
wpop=hwpop/HBAR;
Daco = 7*Q; % acoustic deformation potential, J
egap = 1.424*Q; % energy gap, J
eps_p=1/(1/eps_infty-1/eps_s);
nI=[1e16 1e18 ]*1e6; %density of impurity
Z=1;
q0=sqrt((Q^2*nI)/(kB*T*eps_s));
%%
N=@(E) ((2*meff)^(1.5))*sqrt(E)/(4*pi^(2)*HBAR^(3));
k=@(E) sqrt(2*meff*E)/HBAR;

nE = 200; % number of energy points
vE = linspace(0,1,nE)*Q; % energy axis, J
for ie = 1:nE
E = vE(ie);
W_impurity_16(ie)=(2*pi*nI(1)*Z^2*Q^4*N(E))/((HBAR*eps_s^(2))...
*(q0(1)^(2)*(4*k(E)^2+q0(1)^(2))));
W_impurity_18(ie)=(2*pi*nI(2)*Z^2*Q^4*N(E))/((HBAR*eps_s^(2))...
*(q0(2)^(2)*(4*k(E)^2+q0(2)^(2))));

end

figure(1)
plot(vE/Q, W_impurity_16,'k','linewidth',2)
hold on
plot(vE/Q,W_impurity_18,'r','linewidth',2)
set(gca,'FontSize',14,'FontName','Arial','box','on')
ylabel('scattering rate, 1/s'), xlabel('Energy, eV')
legend('1x10^{16}','1x10^{18}')
```

Appendix B

Solving the Boltzmann Equation - MATLAB code

B.1 Mobility of GaAs in the Relaxation Time Approximation

```
syms x k q0
f = (1-x)/(2*k^2*(1-x)+q0^2)^2; %integrand of eq.2.2
res=int(f,x);
simplify(res); %result of eq.2.2

% constants
c_light = 2.99792458e+8; % light velocity, m/s
H = 6.626070040e-34; % Planck constant, J*s
HBAR = 1.054D-34; % reduced Planck constant, J*s
kB = 1.3806488e-23; % Boltzmann constant, J/K
Q = 1.6021766208e-19; % elementary charge, C
%T = 300; % temperature, K
eps0 = 8.854D-12; % vacuum permittivity constant, F/m
M0 = 9.1095D-31; % electron mass, kg
rho = 5320; % mass density, kg/m^3
eps_s = 13.5*eps0; % static dielectric constant, F/m
eps_infty = 10.9*eps0; % high-frequency dielectric constant, F/m
v_l = 5240; % longitudinal sound velocity, m/s
meff = 0.067*M0; % effective mass, kg
alpha = 0.64/Q; % nonparabolicity factor, 1/J
hwpop = 0.0354*Q; % longitudinal optical phonon energy, J
Daco = 7*Q; % acoustic deformation potential, J
egap = 1.424*Q; % energy gap, J
%% mu_aco
N=@(E) ((2*meff)^(1.5))*sqrt(E)/(4*pi^(2)*HBAR^(3));
f_m=@(E,T) exp(-E/(kB*T));

nE = 1000; % number of energy points
vE = linspace(1e-4,1,nE)*Q; % energy axis, J
vE = vE';
Tmin = 8;
Tmax = 1000;
T = linspace(Tmin,Tmax,100);

Waco_elastic = 2*pi*Daco^2*kB/(HBAR*v_l^(2)*rho)*N(vE)*T;
tau_aco(:,:) = 1./Waco_elastic(:,:);
```

```
mu_aco = zeros(1,length(T));
coeff_mobility = @(T) 2*Q/(meff*3*kB*T);
for i = 1:length(T)
mu_aco(i) = 2*Q./(meff*3*kB*T(i)).*trapz(vE,f_m(vE,T(i)).*vE.*tau_aco(:,i).*N(vE))...
./trapz(vE,f_m(vE,T(i)).*N(vE));
end
figure,
loglog(T,mu_aco,'r--','DisplayName','acoustic elast. d.p.')
hold on
%% mu impurity
nI=1e14*1e6; %density of impurity
Z=1;
k=sqrt(2*meff*vE)/HBAR;
q0=sqrt((Q^2*nI)./(kB*T*eps_s));

x=linspace(-1,1,100);
integral_symbolic = zeros(length(vE),length(T));
for i = 1:length(vE)
k_sym=k(i);
for j = 1:length(T)
q0_sym = q0(j);
integral_symbolic(i,j) = -1/(4*k_sym^4)+1/(4*k_sym^4)*...
log(1+4*k_sym^2/q0_sym^2); %see integral at the beginning of the code
end
end
coeff_impurity=pi*nI*Z^2*Q^4/(HBAR*eps_s^2)*N(vE);
tau_imp = (coeff_impurity.*integral_symbolic(:,1:end)).^(-1);
mu_imp = zeros(1,length(T));
for i = 1:length(T)
mu_imp(i) = 2*Q./(meff*3*kB*T(i)).*trapz(vE,f_m(vE,T(i)).*vE.*tau_imp(:,i).*N(vE))...
./trapz(vE,f_m(vE,T(i)).*N(vE));
end
loglog(T,mu_imp,'b--','DisplayName','ionized impurity')
hold on
%% Matthiessen's rule
mu_0 = (mu_imp.^(-1)+mu_aco.^(-1)).^-1;
loglog(T,mu_0,'k','DisplayName','total (except Jacoboni one)');
legend
xlabel('Temperature [K]');
ylabel('mobility [m^2/(s \cdot V)]')
title(['nI = ' num2str(nI) ' m^{-3}'])
%% Jacoboni approximated formula
energy0 = HBAR.^2*q0.^2/(2*meff);
F_bh = log(1+12*kB*T./energy0)-12*kB*T./energy0./(1+12*kB*T./energy0);
mu_jacoboni = 64*eps_s^2/sqrt(meff)*sqrt(pi)./(nI*Q^3*F_bh).*(2*kB*T).^(3/2);
loglog(T,mu_jacoboni,'g--','DisplayName','ionized impurity [Jacoboni, 11.49]')
```

B.2 Monte Carlo code - tabulated version

```
%main Monte Carlo
```

```
clear
close all
T = 300; % temperature, K
HBAR = 1.054D-34; % reduced Planck constant, J*s
kB = 1.3806488e-23; % Boltzmann constant, J/K
Q = 1.6021766208e-19; % elementary charge, C
eps0 = 8.854D-12; % vacuum permittivity constant, F/m
eps_s = 12.9*eps0; % static dielectric constant, F/m
hwpop = 0.0354*Q; % longitudinal optical phonon energy, J
homega_ij = 0.0278*Q; % longitudinal optical scattering for intervalley
dEgammaL = 0.29*Q; %energy difference between L-Gamma valleys

%for polar optical scattering
B=bernoulli(sym(1:10));
z=sym('z','real');
x=sym('x','real');
nphon=1/z-1/2;
for m=1:5
nphon = nphon + B(2*m)*z^(2*m-1)/factorial(2*m);
end
z=(hwpop)/(kB*T);
Nq=double(subs(nphon)); %well approximates the exact form

%rotation matrix
R = @(kx,ky,kz) [ky/sqrt(kx^2+ky^2), ...
kx*kz/(sqrt(kx^2+ky^2+kz^2)*sqrt(kx^2+ky^2)), ....
kx/sqrt(kx^2+ky^2+kz^2); ...
-kx/sqrt(kx^2+ky^2), ...
ky*kz/(sqrt(kx^2+ky^2+kz^2)*sqrt(kx^2+ky^2)), ...
ky/sqrt(kx^2+ky^2+kz^2); ...
0, ...
-sqrt(kx^2+ky^2)/sqrt(kx^2+ky^2+kz^2), ...
kz/sqrt(kx^2+ky^2+kz^2)];

%%% preparing scattering rates
nI = 1e20; %impurity concentration in m^-3
q0=sqrt((Q^2*nI)/(kB*T*eps_s));
N = 1e3; % accuracy energy span
E_max = 0.5; % in eV
vE = Q*linspace(0,E_max,N);
Wmatrix = zeros(6,length(vE),2); %1st dim. different scatt.rates, 2nd dim.
%energy value and 3rd dim the valley

% GAMMA valley
iv = 1;
for i =1:length(vE)
%emission and absorption, respectively
[Wmatrix(1,i,iv),Wmatrix(2,i,iv)] = pop_scat(vE(i),T,iv,Nq);
[Wmatrix(3,i,iv)] = aco_scat(vE(i),T,iv);
[Wmatrix(4,i,iv)] = imp_scat(vE(i),T,iv,nI);
[Wmatrix(5,i,iv),Wmatrix(6,i,iv)] = iv_scat(vE(i),T,iv);
```

```
end

%L valley
iv = 2;
for i =1:length(vE)
%emission and absorption, respectively
[Wmatrix(1,i,iv),Wmatrix(2,i,iv)] = pop_scat(vE(i),T,iv,Nq);
[Wmatrix(3,i,iv)] = aco_scat(vE(i),T,iv);
[Wmatrix(4,i,iv)] = imp_scat(vE(i),T,iv,nI);
[Wmatrix(5,i,iv),Wmatrix(6,i,iv)] = iv_scat(vE(i),T,iv);
end
Lmatrix = cumsum(Wmatrix,1); %cumulative sum over the first dimension
%% Monte Carlo
close all
tic
nF = 100; %accuracy span over electric field
vF = linspace(0.1,50,nF)*1e5; %vector of electric fields [V/m]
%vF = 10e5;
tau_sim = 1e-9; % simulation time, s
tau = 1e-16; % flight time, s
time = 0:tau:tau_sim; % time axis, s
nt = length(time);

mean_E_final = zeros(1,nF); %average energy @F
mean_v_final = zeros(1,nF); %average velocity @F
occup_gamma = zeros(1,nF); %counts the fraction of time the electron is
%gamma for each EL.FIELD cycle
vector_std_E = zeros(1,nF); %standard deviation for E
vector_std_v = zeros(1,nF); % standard deviation for v
vector_D=zeros(1,nF); %diffusivity


for jj = 1:nF
F = vF(jj); % electric field along the x-axis, V/m
DeltaE = zeros(1,nt); %variations of energy for each electric field
mean_v_tau = zeros(1,nt); %mean carrier velocity during each flight
%time
E_tau = zeros(1,nt); % average energy during drift

kx = 0; ky = 0; kz = 0; % initial state (step 1)
iv = 1;
flag_gamma = 0; %counts how many times in gamma for each TIME cycle
for ii = 1:nt
flag_gamma = flag_gamma + isequal(iv,1);
t = time(ii);
Ei = k2engy(kx,ky,kz,iv);

% move particle in k-space (step 3)
kx = kx -Q*F*tau/HBAR;
% collect statistics (step 4)
Ef = k2engy(kx,ky,kz,iv);
```

```
DeltaE(ii) = Ef - Ei; % energy variation during drift
E_tau(ii) = (Ei + Ef)/2; % average energy during drift
mean_v_tau(ii) = - DeltaE(ii)/(Q*F*tau); %average velocity during
%drift

%%% choose scattering mechanim and select final state (step 5,6)
[value, idx] = min(abs(vE-Ef)); %to find closest energy element
Ef = vE(idx);
r = rand; % pick a random number
norm_ki = norm([kx,ky,kz]); %initial k vector of electron AFTER
%drift, BEFORE scattering
phi = 2*pi*rand;
r_theta = rand;

flag_scat = 1;
if(r < Lmatrix(1,idx(1),iv)*tau)  % select polar optical emission
f = 2*sqrt(Ef*(Ef-hwpop))/(sqrt(Ef)-sqrt(Ef-hwpop)).^2;
cos_theta = ((1+f)-(1+2*f)^r_theta)/f;
norm_kf = engy2k(Ef-hwpop,iv); %minus energy optical phonon em.

elseif(r < Lmatrix(2,idx(1),iv)*tau)  % select polar optical abs.
f = 2*sqrt(Ef*(Ef+hwpop))/(sqrt(Ef)-sqrt(Ef+hwpop)).^2;
cos_theta = ((1+f)-(1+2*f)^r_theta)/f;
norm_kf = engy2k(Ef+hwpop,iv); %plus optical phonon abs.

elseif(r < Lmatrix(3,idx(1),iv)*tau)  % select acoustic scattering
cos_theta = 1-2*r_theta;
norm_kf = norm_ki;

elseif (r < Lmatrix(4,idx(1),iv)*tau) %impurity scattering
cos_theta = 1-2*r_theta/(1+(1-r_theta)*(2*norm_ki/q0)^2);
norm_kf = norm_ki;

%intervalley emission optical
elseif (r < Lmatrix(5,idx(1),iv)*tau) %intervalley emission optical
cos_theta = 1-2*r_theta;
iv = 1.*(iv==2) + 2.*(iv ==1);
norm_kf = engy2k(Ef-homega_ij+dEgammaL*isequal(iv,1)...
-dEgammaL*isequal(iv,2),iv); %energy optical phonon
%intervalley absorption optical
elseif (r < Lmatrix(6,idx(1),iv)*tau)
cos_theta = 1-2*r_theta;
iv = 1.*(iv==2) + 2.*(iv ==1);
norm_kf = engy2k(Ef+homega_ij+dEgammaL*isequal(iv,1)...
-dEgammaL*isequal(iv,2),iv); %energy optical phonon

else % no scattering has occured
flag_scat = 0;
end

if flag_scat
```

```
theta = acos(cos_theta);
%updating k_out in laboratory frame
k_out = R(kx,ky,kz)*[norm_kf*sin(theta)*cos(phi);...
norm_kf*sin(theta)*sin(phi); norm_kf*cos(theta)];
kx = k_out(1);
ky = k_out(2);
kz = k_out(3);
end

end % end of for loop for one F

%%% average energy
mean_E_t = cumsum(E_tau)*tau./time;
mean_E_final(jj) = mean_E_t(end);
%we pick last 90% of simulation to evaluate std
vector_std_E(jj)= std(mean_E_t(floor(nt/10):end));

%%% average velocity
mean_v_t = -cumsum(DeltaE)./(Q*F*time); % diffusion: we use it ...
%for avg time up to simulation time step
mean_v_final(jj) = mean_v_t(end);
%we pick last 90% of simulation to evaluate std
vector_std_v(jj) = std(mean_v_t(floor(nt/10):end));
occup_gamma(jj) = flag_gamma/nt;

%%% noise diffusivity
delta_v= mean_v_tau-mean_v_t; % v(t)-<v(t>
delta_v=delta_v(2:end); %at time 0 the first average value is Inf
MAXLAG = 20000;
[Cv,lags] = xcorr(delta_v,delta_v,MAXLAG);
vector_D(jj) = trapz(lags(MAXLAG+1:end)*tau,Cv(MAXLAG+1:end)...
/length(delta_v)); % length(delta_v) normalization of xcorr

disp(['Progress ' num2str(jj/nF*100) '%'])
end
toc
%% plotting mean energy vs electric field, velocity vs electric field,
% occupancies in valleys

figure(1),
%if ones want to plot without errorbar, uncomment the following
%plot(vF/1e5,mean_E_final/Q*1000,'DisplayName','Average energy');
errorbar(vF/1e5,mean_E_final/Q*1000+dEgammaL/Q*1000*(1-occup_gamma),...
vector_std_E/Q*1000,'DisplayName','Average energy');
ylabel('Electron energy [meV]');
xlabel('Electric field [kV/cm]');
legend

figure(2),
%if ones want to plot without errorbar, uncomment the following
%plot(vF/1e5,abs(mean_v_final*100),'DisplayName','Average velocity');
```

```
errorbar(vF/1e5,abs(mean_v_final*100),abs(vector_std_v*100),...
'DisplayName','Average velocity');
ylabel('velocity [cm/s]');
xlabel('Electric field [kV/cm]');
legend

figure(3),
plot(vF/1e5,occup_gamma,'DisplayName','\Gamma Valley');
hold on
plot(vF/1e5,1-occup_gamma,'DisplayName','L Valley');
hold off
ylabel('Electron occupancy');
xlabel('Electric field [kV/cm]');
legend
%% diffusivity
figure(4),
plot(vF/1e5,vector_D*1e4,'DisplayName','Diffusivity');
xlabel('Electric field [kV/cm]');
ylabel('Diffusivity [cm^2/s]');
legend
%% mobility: Monte Carlo vs relax. time (without pol. opt.scatt)
%from script relaxation time, one gets 15.55 m^2/(V*s) at 298 K.
figure(5),
mu_relax = 15.55;
mu_diff=vector_D/0.0259; % dividing by kB T/q
mu_MC = abs(mean_v_final)./vF;
semilogy(vF/1e5,mu_MC*1e4,'DisplayName','MC mobility');
hold on
semilogy(vF/1e5,ones(1,nF)*mu_relax*1e4,'m','DisplayName','rel.time mobility');
semilogy(vF/1e5,mu_diff*1e4,'r','DisplayName','mobility from diffusivity');
hold off
xlabel('Electric field [kV/cm]');
ylabel('Mobility [cm^2/(V\cdots)]');
legend
```

B.3 Scattering rate functions for Monte Carlo code

B.3.1 Acoustic deformation potential scattering

```
function [W_aco] = aco_scat(Ef,T,iv)
%for elastic acoustisc scattering in Monte Carlo in NON-PARABOLIC approx.
% iv identifies the zone: 1 -- > Gamma, 2 --> L
%costants from appendix tomizawa

HBAR = 1.054D-34; % reduced Planck constant, J*s
kB = 1.3806488e-23; % Boltzmann constant, J/K
Q = 1.6021766208e-19; % elementary charge, C
M0 = 9.1095D-31; % electron mass, kg
rho = 5320; % mass density, kg/m^3
v_l = 5240; % longitudinal sound velocity, m/s
Daco = 7*Q; % acoustic deformation potential, J
```

```
if iv==1
meff = 0.067*M0; % effective mass, kg
alpha = 0.64/Q; % nonparabolicity factor, 1/J
N=@(E) ((2*meff)^(1.5))*sqrt(E.*(1+alpha*E))/(4*pi^(2)*HBAR^(3)).*(1+2*alpha*E);

else
meff = (1.2*0.2^2)^(1/3)*M0; % effective mass, kg
alpha = 0.46/Q; % nonparabolicity factor, 1/J
N=@(E) ((2*meff)^(1.5))*sqrt(E.*(1+alpha*E))/(4*pi^(2)*HBAR^(3)).*(1+2*alpha*E);

end
W_aco=2*pi*Daco^2*kB*T/(HBAR*v_l^2*rho)*N(Ef);

end
```

B.3.2 Intervalley scattering from Γ to L

```
function [W_em,W_ab] = iv_scat(Ef,T,iv)
%for intervalley inelastic optical scattering in Monte Carlo
%in NON-PARABOLIC approx.
% iv identifies the zone: 1 -- > Gamma, 2 --> L
%costants from and Tomizawa Hess


HBAR = 1.054D-34; % reduced Planck constant, J*s
kB = 1.3806488e-23; % Boltzmann constant, J/K
Q = 1.6021766208e-19; % elementary charge, C
M0 = 9.1095D-31; % electron mass, kg
rho = 5320; % mass density, kg/m^3

Dij=1e+11*Q; %coupling constant gamma-L [J/m]
omega_ij=0.0278*Q/HBAR; % da libro HESS pag.108
Nij=1/(exp((HBAR*omega_ij)/(kB*T))-1);
W_em = 0;
W_ab = 0;
deltaE_ij=0.29*Q; % delta energy gamma-L valleys, J

if iv==1
meff_ij=(1.2*0.2^2)^(1/3)*M0;  %final effective mass in L
alpha = 0.46/Q; % final nonparabolicity factor, 1/J
Zj = 4;
else
meff_ij = 0.067*M0;
alpha = 0.64/Q; % final nonparabolicity factor, 1/J
Zj = 1;

end
coeff=(pi*Dij^2*Zj)/(rho*omega_ij);
```

```
N=@(E) ((2*meff_ij)^1.5)*sqrt(E.*(1+alpha*E))/(4*pi^2*HBAR^3)...
.*(1+2*alpha*E);

if (Ef-HBAR*omega_ij-deltaE_ij>0 && iv == 1)
W_em=coeff*N(Ef-HBAR*omega_ij-deltaE_ij)*(Nij+1);
end
if (Ef>0 && iv == 2)
W_em = coeff*N(Ef-HBAR*omega_ij+deltaE_ij)*(Nij+1);
end
if (Ef+HBAR*omega_ij-deltaE_ij>0 && iv == 1)
W_ab=coeff*N(Ef+HBAR*omega_ij-deltaE_ij)*Nij;
end
if (Ef>0 && iv == 2)
W_ab = coeff*N(Ef+HBAR*omega_ij+deltaE_ij)*Nij;
end
end
```

B.3.3 Polar Scattering by Optical Phonons

```
function [W_em,W_ab] = pop_scat(Ef,T,iv,Nq)
%for polar optical scattering in Monte Carlo in NON-PARABOLIC approx.
% iv identifies the zone: 1 -- > Gamma, 2 --> L
HBAR = 1.054D-34; % reduced Planck constant, J*s
Q = 1.6021766208e-19; % elementary charge, C

M0 = 9.1095D-31; % electron mass, kg
hwpop = 0.0354*Q; % longitudinal optical phonon energy, J
wpop=hwpop/HBAR;
eps0 = 8.854D-12; % vacuum permittivity constant, F/m
eps_s = 12.9*eps0; % static dielectric constant, F/m
eps_infty = 10.9*eps0; % high-frequency dielectric constant, F/m
eps_p=1/(1/eps_infty-1/eps_s);
if iv ==1
alpha = 0.64/Q;
meff = 0.067*M0;
gamma=@(E) E*(1+alpha*E);
else
alpha = 0.46/Q;
meff=(1.2*0.2^2)^(1/3)*M0;

gamma=@(E) (E)*(1+alpha*E);

end
d_gamma=@(E) 1+2*alpha*E;

A_e=@(E) (2*(1+alpha*E)*(1+alpha*(E-hwpop))+alpha*(gamma(E)+...
gamma(E-hwpop)))^2;
A_a=@(E) (2*(1+alpha*E)*(1+alpha*(E+hwpop))+alpha*(gamma(E)+...
gamma(E+hwpop)))^2;
B_e=@(E) -2*alpha*gamma(E)^(0.5)*gamma(E-hwpop)^(0.5)*...
(4*(1+alpha*E)*(1+alpha*(E-hwpop))+alpha*(gamma(E)+gamma(E-hwpop)));
```

```
B_a=@(E) -2*alpha*gamma(E)^(0.5)*gamma(E+hwpop)^(0.5)*...
(4*(1+alpha*E)*(1+alpha*(E+hwpop))+alpha*(gamma(E)+gamma(E+hwpop)));
C_e=@(E) 4*(1+2*alpha*E)*(1+2*alpha*(E-hwpop))*(1+alpha*E)...
*(1+alpha*(E-hwpop));
C_a=@(E) 4*(1+2*alpha*E)*(1+2*alpha*(E+hwpop))*(1+alpha*E)...
*(1+alpha*(E+hwpop));

coeff1=(Q^2*sqrt(meff)*wpop)/(4*pi*eps_p*sqrt(2)*HBAR);
if Ef>hwpop
W_em=(coeff1/sqrt(gamma(Ef)))*d_gamma(Ef-hwpop)*(Nq+1)*...
(1/C_e(Ef))*(A_e(Ef)...
*log(abs((gamma(Ef)^(0.5)+gamma(Ef-hwpop)^(0.5))/...
(gamma(Ef)^(0.5)-gamma(Ef-hwpop)^(0.5))))+B_e(Ef));
else
W_em = 0;
end
if Ef>0
W_ab=(coeff1/sqrt(gamma(Ef)))*d_gamma(Ef+hwpop)*(Nq)*(1/C_a(Ef))...
*(A_a(Ef)*log(abs((gamma(Ef)^(0.5)+gamma(Ef+hwpop)^(0.5))...
/(gamma(Ef)^(0.5)-gamma(Ef+hwpop)^(0.5))))+B_a(Ef));
else
W_ab = 0;
end
end
```

B.3.4 Ionized Impurity scattering

```
function [W_imp] = imp_scat(Ef,T,iv,nI)
%for impurity elastic scattering in Monte Carlo in NON-PARABOLIC approx.
% iv identifies the zone: 1 -- > Gamma, 2 --> L
%nI impurity concentration in m^-3
HBAR = 1.054D-34; % reduced Planck constant, J*s
kB = 1.3806488e-23; % Boltzmann constant, J/K
Q = 1.6021766208e-19; % elementary charge, C
M0 = 9.1095D-31; % electron mass, kg
eps0 = 8.854D-12; % vacuum permittivity constant, F/m
eps_s = 12.9*eps0; % static dielectric constant, F/m

q0=sqrt((Q^2*nI)/(kB*T*eps_s));
Z = 1;
if iv==1
meff = 0.067*M0;
alpha = 0.64/Q; %
N=@(E) ((2*meff)^1.5)*sqrt(E.*(1+alpha*E))/...
(4*pi^2*HBAR^3).*(1+2*alpha*E);

else
meff=(1.2*0.2^2)^(1/3)*M0;  %
alpha = 0.46/Q;
N=@(E) ((2*meff)^(1.5))*sqrt(E.*(1+alpha*E))/...
(4*pi^(2)*HBAR^(3)).*(1+2*alpha*E);
```

```
end
k=@(E) sqrt(2*meff*E.*(1+alpha*E))/HBAR;

W_imp=(2*pi*nI*Z^2*Q^4*N(Ef))/((HBAR*eps_s^2)*(q0^2*(4*k(Ef)^2+q0^2)));
end
```

B.3.5 From kinetic energy to wavevector norm

```
function k = engy2k(E,iv)
% inverse energy dispersion relation
% iv identifies the zone: 1 -- > Gamma, 2 --> L
%k input in m^-1. input energy in J

M0 = 9.1095D-31; % electron mass, kg
HBAR = 1.054D-34; % reduced Planck constant, J*s
meff_G = 0.067*M0;
meff_L = (1.2*0.2^2)^(1/3)*M0;
k =(iv==1) * sqrt(2*meff_G*E/HBAR^2) + ...
(iv==2) * sqrt(2*meff_L*E/HBAR^2);
end
```

B.3.6 From wavevector to kinetic energy

```
function energy = k2engy(kx,ky,kz,iv)
% energy dispersion relation
% iv identifies the zone: 1 -- > Gamma, 2 --> L
%k input in m^-1
M0 = 9.1095D-31; % electron mass, kg
Q = 1.6e-19; %
HBAR = 1.054D-34; % reduced Planck constant, J*s
if iv == 1
meff = 0.067*M0;
alpha = 0.64/Q;
else
meff = (1.2*0.2^2)^(1/3)*M0;
alpha = 0.46/Q;
end
gamma =HBAR^2*(kx^2+ky^2+kz^2)/(2*meff);
energy = 2*gamma./(1+sqrt(1+4*alpha*gamma));
end
```

B.4 Monte Carlo code - non tabulated version

```
%main Monte Carlo
clear
close all
tic
T = 300; % temperature, K
HBAR = 1.054D-34; % reduced Planck constant, J*s
kB = 1.3806488e-23; % Boltzmann constant, J/K
Q = 1.6021766208e-19; % elementary charge, C
```

```
eps0 = 8.854D-12; % vacuum permittivity constant, F/m
eps_s = 12.9*eps0; % static dielectric constant, F/m
hwpop = 0.0354*Q; % longitudinal optical phonon energy, J
dEgammaL = 0.29*Q;

tau_sim = 1e-10; % simulation time, s
tau = 1e-16; % flight time, s
kx = 0; ky = 0; kz = 0; % initial state (step 1)
F = 0.1e5; % electric field along the x-axis, V/m
iv = 1; % valley index (1 -> G, 2 ->L)

nI = 1e20; %impurity concentration in m^-3
time = 0:tau:tau_sim; % time axis, s
nt = length(time);
DeltaE = zeros(1,nt);
mean_v_tau = zeros(1,nt);
E_tau = zeros(1,nt);
q0=sqrt((Q^2*nI)/(kB*T*eps_s));
%for polar optical scattering
B=bernoulli(sym(1:10));
z=sym('z','real');
x=sym('x','real');
nphon=1/z-1/2;
for m=1:5
nphon = nphon + B(2*m)*z^(2*m-1)/factorial(2*m);
end
z=(hwpop)/(kB*T);
Nq=double(subs(nphon)); %well approximates the exact form

R = @(kx,ky,kz) [ky/sqrt(kx^2+ky^2), ...
kx*kz/(sqrt(kx^2+ky^2+kz^2)*sqrt(kx^2+ky^2)), ....
kx/sqrt(kx^2+ky^2+kz^2); ...
-kx/sqrt(kx^2+ky^2), ...
ky*kz/(sqrt(kx^2+ky^2+kz^2)*sqrt(kx^2+ky^2)), ...
ky/sqrt(kx^2+ky^2+kz^2); ...
0, ...
-sqrt(kx^2+ky^2)/sqrt(kx^2+ky^2+kz^2), ...
kz/sqrt(kx^2+ky^2+kz^2)];

for ii = 1:nt
t = time(ii);
Ei = k2engy(kx,ky,kz,iv);
% move particle in k-space (step 3)
kx = kx -Q*F*tau/HBAR;
% collect statistics (step 4)
Ef = k2engy(kx,ky,kz,iv);
DeltaE(ii) = Ef - Ei; % energy variation during drift
E_tau(ii) = (Ei + Ef)/2; % average energy during drift
mean_v_tau(ii) = -DeltaE(ii)/(Q*F*tau);
% choose scattering mechanim and select final state (step 5,6)
[W(1),W(2)] = pop_scat(Ef,T,iv,Nq); %emission and absorption
```

```
[W(3)] = aco_scat(Ef,T,iv);
[W(4)] = imp_scat(Ef,T,iv,nI);
[W(5),W(6)] = iv_scat(Ef,T,iv);
L = cumsum(W);
r = rand; % pick a random number
norm_ki = norm([kx,ky,kz]); %initial k vector of electron AFTER drift, BEFORE scattering
phi = 2*pi*rand;
r_theta = rand;

flag_scat = 1;
if(r < L(1)*tau)  % select polar optical emission
f = 2*sqrt(Ef*(Ef-0.0354*Q))/(sqrt(Ef)-sqrt(Ef-0.0354*Q)).^2;
cos_theta = ((1+f)-(1+2*f)^rand)/f;
norm_kf = engy2k(Ef-0.0354*Q,iv); %energy optical phonon subtracted

elseif(r < L(2)*tau)  % select polar optical absorption
f = 2*sqrt(Ef*(Ef+0.0354*Q))/(sqrt(Ef)-sqrt(Ef+0.0354*Q)).^2;
cos_theta = ((1+f)-(1+2*f)^rand)/f;
norm_kf = engy2k(Ef+0.0354*Q,iv); %energy optical phonon
elseif(r < L(3)*tau)  % select acoustic scattering
cos_theta = 1-2*rand;
norm_kf = norm_ki;
elseif (r < L(4)*tau) %impurity scattering
r_theta=rand;
cos_theta = 1-2*r_theta/(1+(1-r_theta)*(2*norm_ki/q0)^2);
norm_kf = norm_ki;
elseif (r < L(5)*tau) % intervalley emission optical
cos_theta = 1-2*rand;
iv = 1.*(iv==2) + 2.*(iv ==1);
norm_kf = engy2k(Ef-0.0278*Q+dEgammaL*isequal(iv,1)-dEgammaL*isequal(iv,2),iv);
elseif (r < L(6)*tau) % intervalley absorption optical
cos_theta = 1-2*rand;
iv = 1.*(iv==2) + 2.*(iv ==1);
norm_kf = engy2k(Ef+0.0278*Q+dEgammaL*isequal(iv,1)-dEgammaL*isequal(iv,2),iv);
else % no scattering has occured
flag_scat = 0;
end
if flag_scat
theta = acos(cos_theta);
k_out = R(kx,ky,kz)*[norm_kf*sin(theta)*cos(phi);...
 norm_kf*sin(theta)*sin(phi); norm_kf*cos(theta)];
kx = k_out(1);
ky = k_out(2);
kz = k_out(3);
end

end % end of for loop
toc
%% post-processing: convergence, diffusivity, ..
mean_E_t = cumsum(E_tau)*tau./time;
figure(1),
```

```
plot(time*1e12,mean_E_t/Q*1000,'DisplayName','Average cumulative energy');
ylabel('Electron energy [meV]');
xlabel('time [ps]');
legend

mean_v_t = -cumsum(DeltaE)./(Q*F*time);
figure(2),
plot(time*1e12,mean_v_t*100,'DisplayName','Average cumulative velocity');
ylabel('velocity [cm/s]');
xlabel('time [ps]');
legend
%% autocorrelation function
figure(3),
delta_v= mean_v_tau-mean_v_t;
delta_v=delta_v(2:end); %since first element is NaN by dividing 0
MAXLAG = 20000;
[Cv,lags] = xcorr(delta_v,delta_v,MAXLAG);
plot(lags(MAXLAG+1:end)*tau*1e12,Cv(MAXLAG+1:end)/length(delta_v),'ro-');
xlabel('time, ps')
ylabel('Autocorrelation function, m^2/s^2')

%diffusivity
vector_D = trapz(lags(MAXLAG+1:end)*tau,Cv(MAXLAG+1:end)/length(delta_v))
```

B.5 Monte Carlo code for impact ionization - tabulated

```
%main Monte Carlo
clear
close all
T = 300; % temperature, K
HBAR = 1.054D-34; % reduced Planck constant, J*s
kB = 1.3806488e-23; % Boltzmann constant, J/K
Q = 1.6021766208e-19; % elementary charge, C
eps0 = 8.854D-12; % vacuum permittivity constant, F/m
eps_s = 12.9*eps0; % static dielectric constant, F/m
hwpop = 0.0354*Q; % longitudinal optical phonon energy, J
homega_ij = 0.0278*Q; % longitudinal optical scattering for intervalley
dEgammaL = 0.29*Q;

%for polar optical scattering
B=bernoulli(sym(1:10));
z=sym('z','real');
x=sym('x','real');
nphon=1/z-1/2;
for m=1:5
nphon = nphon + B(2*m)*z^(2*m-1)/factorial(2*m);
end
z=(hwpop)/(kB*T);
Nq=double(subs(nphon)); %well approximates the exact form
%rotation matrix
```

```
R = @(kx,ky,kz) [ky/sqrt(kx^2+ky^2), ...
kx*kz/(sqrt(kx^2+ky^2+kz^2)*sqrt(kx^2+ky^2)), ....
kx/sqrt(kx^2+ky^2+kz^2); ...
-kx/sqrt(kx^2+ky^2), ...
ky*kz/(sqrt(kx^2+ky^2+kz^2)*sqrt(kx^2+ky^2)), ...
ky/sqrt(kx^2+ky^2+kz^2); ...
0, ...
-sqrt(kx^2+ky^2)/sqrt(kx^2+ky^2+kz^2), ...
kz/sqrt(kx^2+ky^2+kz^2)];

% preparing scattering rates
nI = 1e20; %impurity concentration in m^-3
q0=sqrt((Q^2*nI)/(kB*T*eps_s));
N = 1e3;
E_max = 2.5; % in eV
vE = Q*linspace(0,E_max,N);
Wmatrix = zeros(7,length(vE),2); %1st dim. different scatt.rates, 2nd dim. energy value and
%for impact ionization coefficients
Eth = 1.7*Q; %energy J,
S = 2.5e15; % s^-1
Egap = 1.441*Q; %for GaAs, @300 K
idx_gap = find((vE-Egap).*(vE-Egap>0),1); %finds the idx in vE
 %corresponding to energy greater than Egap
idx_Eth = find((vE-Eth).*(vE-Eth>0),1)-1; %finds the idx in
%vE corresponding to largest energy SMALLER than Eth
for i = idx_gap:idx_Eth
Wmatrix(7,i,1) = S*((vE(i)-Eth)/Eth)^2;
Wmatrix(7,i,2) = Wmatrix(7,i,1); %equal scattering rates because it depends
% on the kinetic energy.
end

% GAMMA valley
iv = 1;
for i =1:length(vE)
[Wmatrix(1,i,iv),Wmatrix(2,i,iv)] = pop_scat(vE(i),T,iv,Nq); %emission and absorption
[Wmatrix(3,i,iv)] = aco_scat(vE(i),T,iv);
[Wmatrix(4,i,iv)] = imp_scat(vE(i),T,iv,nI);
[Wmatrix(5,i,iv),Wmatrix(6,i,iv)] = iv_scat(vE(i),T,iv);
end
%L valley
iv = 2;
for i =1:length(vE)
[Wmatrix(1,i,iv),Wmatrix(2,i,iv)] = pop_scat(vE(i),T,iv,Nq); %emission and absorption
[Wmatrix(3,i,iv)] = aco_scat(vE(i),T,iv);
[Wmatrix(4,i,iv)] = imp_scat(vE(i),T,iv,nI);
[Wmatrix(5,i,iv),Wmatrix(6,i,iv)] = iv_scat(vE(i),T,iv);
end
Lmatrix = cumsum(Wmatrix,1);
%% Monte Carlo
close all
tic
```

```
nF = 6;
vF = linspace(25,66,nF)*1e6;
tau_sim = 1e-9; % simulation time, s
tau = 1e-16; % flight time, s
time = 0:tau:tau_sim; % time axis, s
nt = length(time);

mean_E_final = zeros(1,nF);
mean_v_final = zeros(1,nF);
occup_gamma = zeros(1,nF); %counts the fraction of time the electron is gamma @F
vector_std_E = zeros(1,nF);
vector_std_v = zeros(1,nF);
vector_D=zeros(1,nF); %diffusivity

v_mean_alpha = zeros(1,nF); %impact ioniz.
v_std_alpha = zeros(1,nF); %impact ioniz.
for jj = 1:nF
F = vF(jj); % electric field along the x-axis, V/m
DeltaE = zeros(1,nt);
mean_v_tau = zeros(1,nt);
E_tau = zeros(1,nt);

kx = 0; ky = 0; kz = 0; % initial state (step 1)
iv = 1;
flag_gamma = 0; %counts how many times the electron is gamma for each TIME cycle
tot_path = 0;
count_impact = 0;
mean_free_path = zeros(1,nt);
for ii = 1:nt
flag_gamma = flag_gamma + isequal(iv,1);
t = time(ii);
Ei = k2engy(kx,ky,kz,iv);
% move particle in k-space (step 3)
kx = kx -Q*F*tau/HBAR;
% collect statistics (step 4)
Ef = k2engy(kx,ky,kz,iv);
DeltaE(ii) = Ef - Ei; % energy variation during drift
E_tau(ii) = (Ei + Ef)/2; % average energy during drift
mean_v_tau(ii) = - DeltaE(ii)/(Q*F*tau);
tot_path = tot_path + abs(mean_v_tau(ii)*tau);
% choose scattering mechanim and select final state (step 5,6)
[value, idx] = min(abs(vE-Ef));
Ef = vE(idx);
r = rand; % pick a random number
norm_ki = norm([kx,ky,kz]); %initial k vector of electron AFTER drift, BEFORE scattering
phi = 2*pi*rand;
r_theta = rand;

flag_scat = 1;
if(r < Lmatrix(1,idx(1),iv)*tau)  % select polar optical emission
f = 2*sqrt(Ef*(Ef-0.0354*Q))/(sqrt(Ef)-sqrt(Ef-0.0354*Q)).^2;
```

```
cos_theta = ((1+f)-(1+2*f)^r_theta)/f;
norm_kf = engy2k(Ef-0.0354*Q,iv);

elseif(r < Lmatrix(2,idx(1),iv)*tau)  % select polar optical absorption
f = 2*sqrt(Ef*(Ef+0.0354*Q))/(sqrt(Ef)-sqrt(Ef+0.0354*Q)).^2;
cos_theta = ((1+f)-(1+2*f)^r_theta)/f;
norm_kf = engy2k(Ef+0.0354*Q,iv);

elseif(r < Lmatrix(3,idx(1),iv)*tau)  % select acoustic scattering
cos_theta = 1-2*r_theta;
norm_kf = norm_ki;

elseif (r < Lmatrix(4,idx(1),iv)*tau) %impurity scattering
cos_theta = 1-2*r_theta/(1+(1-r_theta)*(2*norm_ki/q0)^2);
norm_kf = norm_ki;

elseif (r < Lmatrix(5,idx(1),iv)*tau) % intervalley emission optical
cos_theta = 1-2*r_theta;
iv = 1.*(iv==2) + 2.*(iv ==1);
norm_kf = engy2k(Ef-0.0278*Q+dEgammaL*isequal(iv,1)-dEgammaL*isequal(iv,2),iv);
elseif (r < Lmatrix(6,idx(1),iv)*tau) % intervalley absorption optical
cos_theta = 1-2*r_theta;
iv = 1.*(iv==2) + 2.*(iv ==1);
norm_kf = engy2k(Ef+0.0278*Q+dEgammaL*isequal(iv,1)-dEgammaL*isequal(iv,2),iv);
elseif (r < Lmatrix(7,idx(1),iv)*tau) %impact ionization
cos_theta = 1-2*r_theta; %being isotropic, [30,pag.5]
iv = randi([1 2],1); %see [30,pag.5];
norm_kf = engy2k(Ef-Egap,iv);
if count_impact == 0
mean_free_path(1) = tot_path;
count_impact = 1;
else
count_impact = count_impact+1;
mean_free_path(count_impact) = tot_path-sum(mean_free_path(1:count_impact-1));
end
else % no scattering has occured
flag_scat = 0;
end
if flag_scat
theta = acos(cos_theta);
k_out = R(kx,ky,kz)*[norm_kf*sin(theta)*cos(phi);
... norm_kf*sin(theta)*sin(phi); norm_kf*cos(theta)];
kx = k_out(1);
ky = k_out(2);
kz = k_out(3);
end

end % end of for loop
%average energy
mean_E_t = cumsum(E_tau)*tau./time;
mean_E_final(jj) = mean_E_t(end);
```

```
vector_std_E(jj)= std(mean_E_t(floor(nt/10):end));

%average velocity
mean_v_t = -cumsum(DeltaE)./(Q*F*time); % diffusion: we use it for avg time
% up to simulation time step
mean_v_final(jj) = mean_v_t(end);
vector_std_v(jj) = std(mean_v_t(floor(nt/10):end));
occup_gamma(jj) = flag_gamma/nt;
%impact ionization
mean_free_path = mean_free_path((mean_free_path>0)); % to remove the 0 tail
v_alpha = 1./mean_free_path(floor(length(mean_free_path)/10):end);
v_mean_alpha(jj) = mean(v_alpha);

disp(['Progress ' num2str(jj/nF*100) '%'])
end
toc
%% plotting mean energy vs electric field, velocity vs electric field,
%occupancies in valleys
figure(1),
%plot(vF/1e5,mean_E_final/Q*1000,'DisplayName','Average energy');
errorbar(vF/1e5,mean_E_final/Q*1000,vector_std_E/Q*1000,...
'DisplayName','Average energy');
ylabel('Electron energy [meV]');
xlabel('Electric field [kV/cm]');
legend

figure(2),
%plot(vF/1e5,abs(mean_v_final*100),'DisplayName','Average velocity');
errorbar(vF/1e5,abs(mean_v_final*100),abs(vector_std_v*100),'DisplayName',...
'Average velocity');
ylabel('velocity [cm/s]');
xlabel('Electric field [kV/cm]');
legend
%% impact ionization coefficient
figure(6),
plot(1./vF*1e8,v_mean_alpha,'DisplayName','Electrons');
xlabel('E^{-1} [10^{-8} m/V]');
ylabel('Ionization rate (m^{-1})');
legend
```

Bibliography

[1] F. Bertazzi and M. Goano, *Monte Carlo modeling of carrier transport in crystalline materials: Electronic properties of materials - Lab 2*. Lecture Notes, March 2019.

[2] K. Tomizawa, *Numerical Simulation of Submicron Semiconductor Devices*. Boston: Artech House, 1993.

[3] C. Jacoboni, *Theory of Electron Transport in Semiconductors. A Pathway from Elementary Physics to Nonequilibrium Green Functions*. Berlin: Springer-Verlag, 2010.

[4] C. Jacoboni and P.Lugli, *The Monte Carlo Method for Semiconductor Device simulation* ser. Computational Microelectronics. Wien: Springer-Verlag, 1989.

[5] http://www.ioffe.ru/SVA/NSM/Semicond/GaAs/, May 2019.